Crack Width Evaluation of RC Members Reinforced with Braided AFRP Bars

Shuai Hao

(Master's Program in Engineering Mechanics and Energy)

Advised by Toshiyuki Kanakubo

Submitted to the Graduate School of Systems and Information Engineering in Partial Fulfillment of the Requirements for the Degree of Master of Engineering
at the
University of Tsukuba

March 2017

ABSTRACT

The use of AFRP (Aramid Fiber-Reinforced Polymer) bars as an alternative to the steel reinforcements is a feasible scheme to prevent the corrosion of rebar. However, AFRP bars with low elastic modulus and bond stiffness could cause a larger crack width in comparison to steel rebar. It is a critical issue to control cracks of concrete reinforced with AFRP bars. On the other hand, a second differential equation on bond problem which considering bond force equilibrium and slip compatibility condition has been solved as an equation given by relationship between the strain of reinforcement and loaded end slip which is considered as the half of crack width.

This study aims to propose theoretical calculation formulas to predict crack width of RC members reinforced with AFRP bars. Braided AFRP bars with two types of surface treatment, non-coated type and sand-coated one, are focused on in this study. A pullout bond test was conducted for obtaining the bond constitutive law which is considered as the key to propose the formulas. A tensile bond test which can be used to confirm the adaptability of proposed calculation formula was carried out as well.

Two types of tri-linear models for bond constitutive law are proposed based on the experimental results of pullout bond test both for non-coated and sand-coated type AFRP bars. Under the regression analysis of the pullout bond test results, each of the bond stiffness and characteristic value is estimated as a function which is mainly related to concrete strength and bar diameter. The crack width prediction formulas are proposed by using the estimated bond constitutive law. The proposed crack width prediction formulas show good agreements with the experimental crack widths observed in tensile bond test.

CONTENTS

LIST OF FIGURES

CHAPTER 1 Introduction

It is well known that concrete reinforced with steel rebar has long been used as a building construction for its good durability and low cost. However, steel rebar has its own weakness: susceptibility to corrosion. It has seriously impacted the performance of existing buildings safety and cause economic loss due to corrosion-related maintenance. And also, steels are likely to conduct electrical and magnetic fields, those are not desirable in some special building such as power-generation and medical use.

The use of AFRP (Aramid Fiber-Reinforced Polymer) bars as an alternative to the steel reinforcements is a feasible scheme to prevent the corrosion of rebar. It can supplier for concrete applications where the environments prohibit the use of steel owing to its noncorrosive nature and broad resistance to other chemicals[1-1]. Moreover, AFRP bars also have an advantage of lightweight and high strength in comparison to steel.

However, FRP (Fiber-Reinforced Polymer) reinforcements are manufactured from different fibers (carbon, aramid, glass, etc.) with various resins and surface treatments which are different from conventional steel rebar. Due to the lack of well-established standards and variation in their effective parameters, it is difficult to propose a plenary model to predict the bond performance between concrete and each FRP reinforcement. This study only focuses on braided AFRP bars with two types of surface treatment which are non-coated and sand-coated treatment.

AFRP bars with low elastic modulus and bond stiffness may cause a lager crack width of concrete. It is a critical issue to control cracks of concrete reinforced with AFRP bars. The numbers of studies have been conducted regarding the crack width of reinforced concrete members. On those conclusions that bond behavior between reinforcement and concrete controls the crack characteristics of the reinforced concrete members and the bond behavior itself is determined by bond stress and slip relationship (hereinafter, bond constitutive law). Meanwhile, a second differential equation on bond problem which considering bond force equilibrium and slip compatibility condition has been introduced[1-2]. It is expected to be solved as a form given by relationship between the strain of reinforcement and loaded end slip which is consider as the half of crack width[1-3] (Eq. (1)). If the function of bond stress and slip is determined, the crack width prediction formula can be obtained by integral calculus of the Eq. (1). Therefore, a theoretical and general calculation formula to predict crack width of reinforced concrete members has been proposed by using the bi-linear model for bond constitutive law to solve the bond problem equation[1-3].

$$\varepsilon_{bl} = \frac{\phi_b}{\sigma_{ct} \cdot A_c} \int_0^{s_l} \tau_b \cdot ds + \left(\frac{1+n \cdot p}{2}\right) \frac{\sigma_{ct} \cdot A_c}{E_b \cdot A_b} \quad \text{Eq. (1)}$$

where,

ε_{bl} : strain of reinforcement at loaded end

ϕ_b : perimeter of bar, σ_{ct} : tensile strength of concrete

A_c : sectional area of concrete, A_b : sectional area of reinforcement

E_b : elastic modulus of reinforcement, s_l : slip at loaded end

E_c : elastic modulus of concrete, τ_b : bond stress

n : elastic modulus ratio $= E_b/E_c$

p : reinforcement ratio=A_b/A_c

The above equation also includes the elastic modulus which has an influence on the crack width. It is expected to solve the equation by giving the information of bond constitutive law of AFRP bars to obtain a reliable crack width prediction formula for AFRP bar.

This study aims to propose theoretical calculation formulas to predict crack width of RC members reinforced with AFRP bars. In contrast to traditional steel bars, the bond constitutive law should be described by tri-linear model, considering the bond behavior between the AFRP bars and concrete.

Chapter two introduces the outline of experiment and the test results. It includes the method to obtain the bond constitutive law by conducting pullout bond test and the experiment program about tensile bond test which can be used to confirm the adaptability of proposed calculation formulas.

Chapter three introduces the tri-linear model for bond constitutive law based on the test results and the solution result of Eq. (1) by using the proposed constitutive law to give the theoretical calculation formulas.

Chapter four focuses on estimating the parameters of theoretical calculation formulas to make a general prediction formula for braided AFRP bars where the formulas are expected to be given by a function of bar dimeter, compressive strength of concrete and some other constants.

Chapter five presents the general calculation formula for braided AFRP bars based on the parameter estimation in chapter 4 and discusses the adaptability of calculation formula.

Chapter six summarizes this study and presents the conclusions.

CHAPTER 2 Experiment Program

The bond constitutive law is the key component to propose calculation formulas. It should be obtained directly by conducting pullout bond test. And the tensile bond test is also performed to obtain measured crack width in order to compare the experimental results and the calculated ones, which can be used to confirm the adaptability of the proposed calculation formulas. Both two tests are conducted at the same time using same reinforcement and concrete under an assumption that local bond constitutive law in pullout bond test has not changed in the condition of tensile bond test.

2.1 Tested Reinforcement and Concrete

Fig. 2.1 shows the tested reinforcements with two types of surface. One is non-coated type and another one is the sand-coated type. Each type of them includes four different diameters. As shown in Table 2.1, regarding to the mechanical properties of two types of tested reinforcement, there is no difference between the two types if the diameters are same. In addition, the elastic modulus among those four different diameter of bars do not change too much.

There are two series of experiment has been conducted. The first series is for reinforcement with diameter of 8.10mm and 13.51mm. Those concrete target compressive strength was set as 36MPa. The second series of experiment was performed with the specimen reinforced with bar diameter of 9.73mm and 10.95mm.Those concrete target compressive strength was set as 24MPa, 36MPa and 48MPa.

Table 2.2 shows the mechanical properties of concrete. For each series of experiment, same batch of concrete are used for both pullout bond test and tensile bond test.

Non-coated type
(named “RA”)

Sand-coated type
(named “RAS”)

Fig. 2.1 Two types of AFRP bar

Table 2.1 List of reinforcement

Reinforcement	Diameter (mm)	Max. tensile strength (kN)	Elastic modulus (kN/mm^2)
RA7&RA7S	8.10	69	63.7
RA9&RA9S	9.73	100	66.2
RA11&RA11S	10.95	124	66.3
RA13&RA13S	13.51	186	71.2

Table 2.2 Mechanical properties of concrete

Series	Concrete target strength (N/mm^2)	Compressive strength (N/mm^2)	Tensile strength (N/mm^2)	Elastic modulus (kN/mm^2)
1st	36	37.2	2.67	26.9
2nd	24	28.5	2.63	23.8
2nd	36	37.6	3.32	26.3
2nd	48	48.5	3.76	29.5

2.2 Pullout Bond Test

2.2.1 Outline of pullout bond test

Pullout bond test was conducted for obtaining the bond constitutive law between AFRP bar and concrete directly.

Table 2.3 shows the list of specimens. Three same specimens for each parameter were tested.
Fig. 2.2 shows the detail of test specimens. It is a rectangular concrete block with height of 100mm. The sectional size of the concrete block in first series are varying as 80x80mm, 100x100mm and 120x120mm. The sectional size of the concrete in second series was set as 100x100mm.

One AFRP bar is arranged in the central position of the concrete block. Unbonded region is set at the both loaded and free end with length of 4 times bar diameter, d_b. Teflon sheet was placed between specimen and steel plate to avoid the restriction of lateral displacement of concrete block. One LVDT was set at the free end of concrete block to measure slip at free end. The loaded end slip is calculated as the elongation of reinforcement added to the free end slip under the assumption that bond stress distributes uniformly among the bonded region. Fig .2.3 shows a photo of specimen.

Each specimen was subjected to the monotonic pullout load until the slippage of reinforcement reached to 20 mm or concrete failed by splitting.

Table 2.3 (a) List of specimens of first series

Specimen ID	Reinforcement	Concrete sectional size (mm x mm)	Bonded region (mm)	Number of specimens
P80RA7	RA7	80x80	32	3
P100RA7		100x100		3
P120RA7		120x120		3
P80RA7S	RA7S	80x80		3
P100RA7S		100x100		3
P120RA7S		120x120		3
P80RA13	RA13	80x80	52	3
P100RA13		100x100		3
P120RA13		120x120		3
P80RA13S	RA13S	80x80		3
P100RA13S		100x100		3
P120RA13S		120x120		3

Table 2.3 (b) List of specimens of second series

Specimen ID	Reinforcement	Concrete target strength (N/mm^2)	Bonded region (mm)	Number of specimens
C24RA9	RA9	24	36	3
C24RA11	RA11		44	3
C24RA9S	RA9S		36	3
C24RA11S	RA11S		44	3
C36RA9	RA9	36	36	3
C36RA11	RA11		44	3
C36RA9S	RA9S		36	3
C36RA11S	RA11S		44	3
C48RA9	RA9	48	36	3
C48RA11	RA11		44	3
C48RA9S	RA9S		36	3
C48RA11S	RA11S		44	2*

*: One of the specimen was not cast appropriately (the free end of AFRP bar was not outside of concrete block, LVDT cannot measure the slippage of bar)

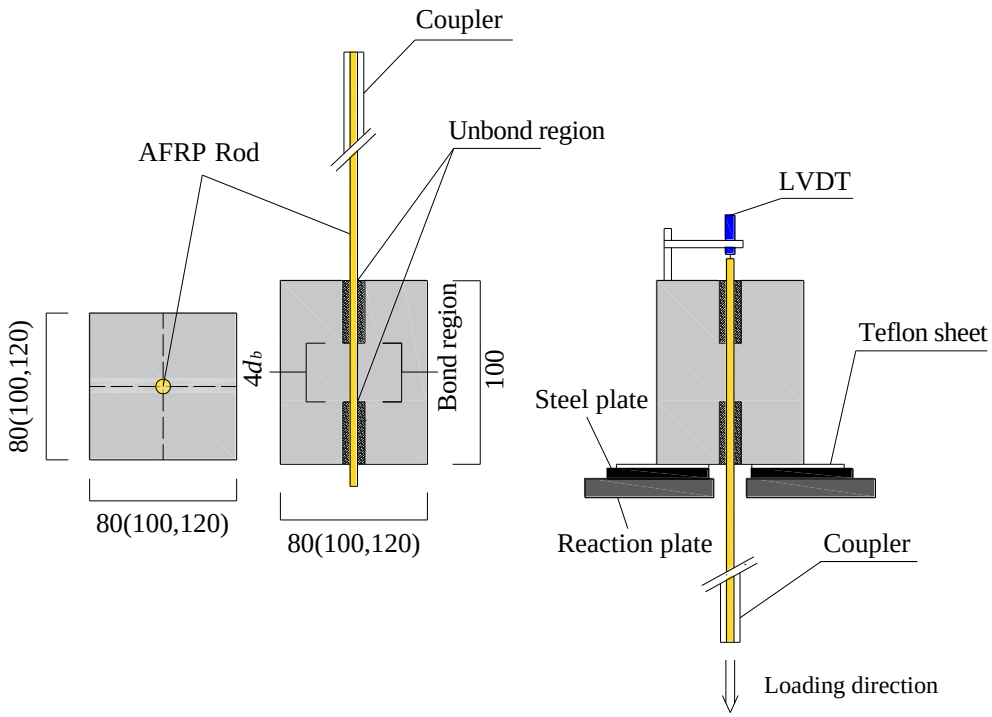

Fig. 2.2 Details of specimens and loading method of pullout bond test

Fig. 2.3 Photo of pullout bond test specimen

2.2.2 Test results of pullout bond test

Table 2.4 shows the test results of pullout bond test for specimen of both two types. The sectional size of concrete does not have a large influence to the max. bond stress and its corresponding slippage. For those specimens reinforced with sand-coated type bar, the stiff resistance is provided by bearing between sand and concrete. When this resistance fails, the bar starts slipping with a sudden fall of bond stress. The bond stress at where the bar starts slipping is defined as “slipping bond stress” in this study. Fig. 2.4 shows the example of bond stress-slip relationship of sand-coated type bar and the definition of slipping bond stress.

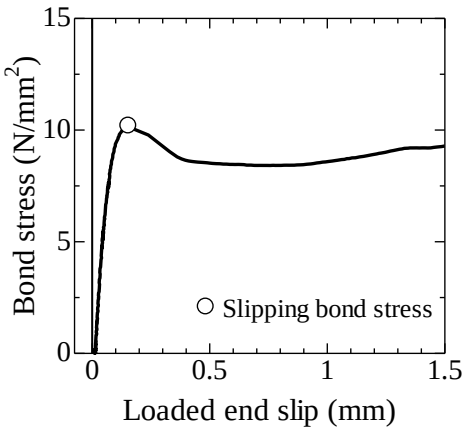

Fig. 2.4 Example of bond stress – slip relationship of sand-coated type bar

Basically, as the bar diameter increasing, concrete is more likely failed by splitting. Regarding to the specimen reinforced with non-coated type bar, the max. bond stress of those splitting specimens were not obtained. On the other hand, although several specimens reinforced with sand-coated type bar failed by concrete splitting, the slipping bond stress was obtained because the splitting failure occurred during the second or third increase branch of bond stress and it is far away from the slip at the slipping bond stress.

Fig. 2.5 shows the bond stress and slip relationship for each specimen. It can be found that the surface treatment of AFRP braided bar determines the characteristic of bond constitutive law. Sand coated type shows higher bond stiffness than that of non-coated. However, regardless of the surface treatment of those two types, the max. bond stress are similar. For both two types, after reaching the first peak of bond stress there is a decrease branch. At the end of decrease branch, the bond stress will increase again. This is considered that the lugs as the surface shape of braided bars move toward to loaded end will cause a new mechanical occlusion between the reinforcement and concrete.

In addition, for predicting the crack width, the whole bond constitutive law from 0 to 20mm is not necessary. Fig. 2.5 also shows a relative small range of the bond constitutive law which is set as 8mm for non-coated type and 3mm for sand-coated type, respectively.

Table 2.4 (a) Test results of pullout bond test (non-coated type, first series)

Specimen ID	Sectional size (mm x mm)	Max. bond stress (N/mm^2)	Slip at max. bond stress (mm)	Failure mode
P80RA7-1	80x80	11.22	4.90	Pullout
P80RA7-2		11.77	5.02	
P80RA7-3		10.73	5.20	
P80RA13-1		9.71	1.97	Concrete splitting
P80RA13-2		8.75	3.63	
P80RA13-3		8.52	2.86	
P100RA7-1	100x100	10.83	4.37	Pullout
P100RA7-2		12.37	3.84	
P100RA7-3		13.31	4.13	
P100RA13-1		11.00	2.56	Concrete splitting
P100RA13-2		11.47	3.68	
P100RA13-3		9.27	2.53	
P120RA7-1	120x120	13.19	4.80	Pullout
P120RA7-2		13.34	4.63	
P120RA7-3		14.22	3.10	
P120RA13-1		9.86	3.53	Concrete splitting
P120RA13-2		12.10	4.35	
P120RA13-3		11.10	3.01	

Table 2.4 (b) Test results of pullout bond test (sand-coated type, first series)

Specimen ID	Sectional size (mm x mm)	Slipping bond stress (N/mm^2)	Slip at slipping bond stress (mm)	Failure mode
P80RA7S-1	80x80	11.50	0.12	Pullout
P80RA7S-2		12.26	0.12	
P80RA7S-3		13.45	0.23	Concrete splitting
P80RA13S-1		10.23	0.15	Pullout
P80RA13S-2		10.05	0.16	
P80RA13S-3		10.84	0.16	
P100RA7S-1	100x100	10.76	0.12	
P100RA7S-2		10.39	0.14	
P100RA7S-3		10.12	0.19	
P100RA13S-1		8.73	0.18	
P100RA13S-2		9.77	0.24	
P100RA13S-3		7.94	0.14	
P120RA7S-1	120x120	11.50	0.33	
P120RA7S-2		11.29	0.18	
P120RA7S-3		9.22	0.17	
P120RA13S-1		11.32	0.21	
P120RA13S-2		10.97	0.17	
P120RA13S-3		9.43	0.20	

Table 2.4 (c) Test results of pullout bond test (non-coated type, second series)

Specimen ID	Concrete strength (N/mm^2)	Max. bond stress (N/mm^2)	Slip at max. bond stress (mm)	Failure mode
C24RA9-1	28.5	11.48	4.83	Pullout
C24RA9-2		11.81	4.66	
C24RA9-3		13.31	5.43	
C24RA11-1		14.63	4.85	Concrete splitting
C24RA11-2		14.70	3.34	
C24RA11-3		12.38	2.75	
C36RA9-1	37.6	14.02	4.74	Pullout
C36RA9-2		11.95	4.47	
C36RA9-3		11.13	4.10	
C36RA11-1		12.56	4.59	Concrete splitting
C36RA11-2		13.26	5.65	
C36RA11-3		11.20	5.96	Pullout
C48RA9-1	48.5	10.81	5.68	Pullout
C48RA9-2		15.58	5.23	
C48RA9-3		14.40	6.95	
C48RA11-1		17.02	2.14	Concrete splitting
C48RA11-2		16.48	2.46	
C48RA11-3		17.70	2.89	

Table 2.4 (d) Test results of pullout bond test (sand-coated type, second series)

Specimen ID	Concrete strength (N/mm^2)	Slipping bond stress (N/mm^2)	Slip at slipping bond stress (mm)	Failure mode
C24RA9S-1	28.5	10.23	0.17	Concrete splitting
C24RA9S-2		12.10	0.15	
C24RA9S-3		12.09	0.17	pullout
C24RA11S-1		12.19	0.22	Concrete splitting
C24RA11S-2		12.98	0.20	
C24RA11S-3		12.25	0.25	
C36RA9S-1	37.6	13.89	0.18	Pullout
C36RA9S-2		14.53	0.19	Concrete splitting
C36RA9S-3		11.41	0.12	Pullout
C36RA11S-1		11.26	0.17	Concrete splitting
C36RA11S-2		10.80	0.17	
C36RA11S-3		11.39	0.18	Pullout
C48RA9S-1	48.5	15.22	0.20	Concrete splitting
C48RA9S-2		14.53	0.20	Pullout
C48RA9S-3		16.16	0.16	Concrete splitting
C48RA11S-1		14.76	0.21	
C48RA11S-2		14.00	0.20	

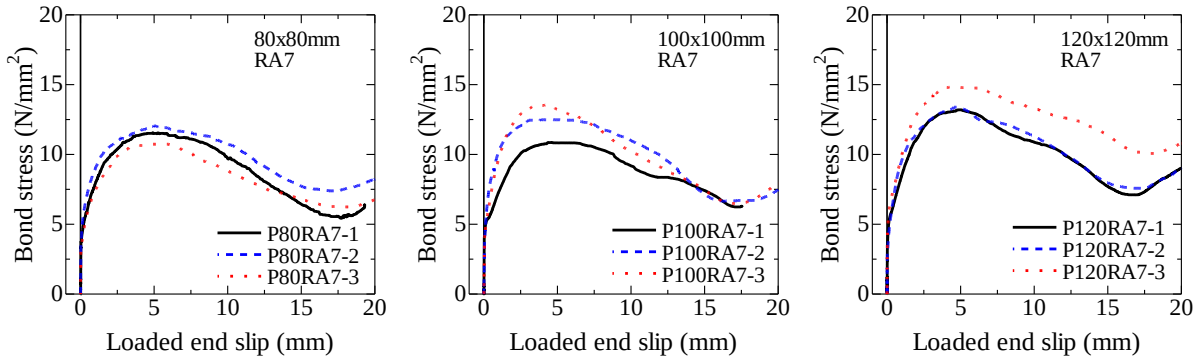

Fig. 2.5 (a) Bond stress – slip relationship (RA7 series)

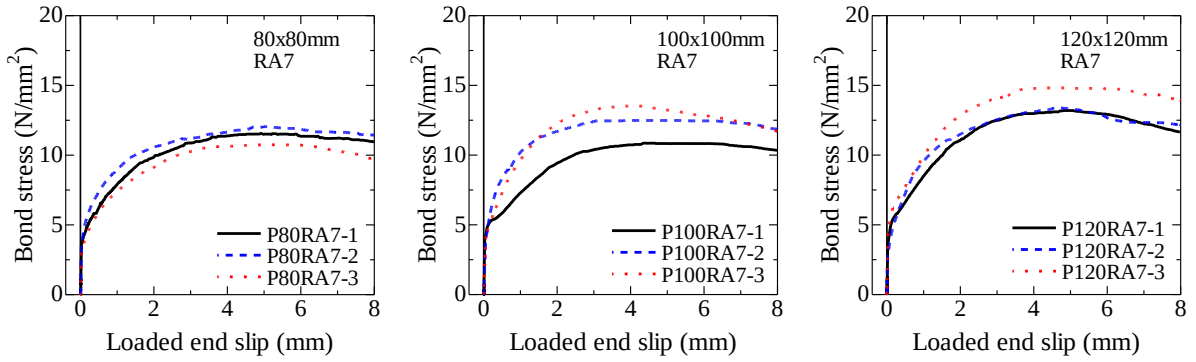

Fig. 2.5 (b) Bond stress – slip relationship (RA7 series, until 8mm)

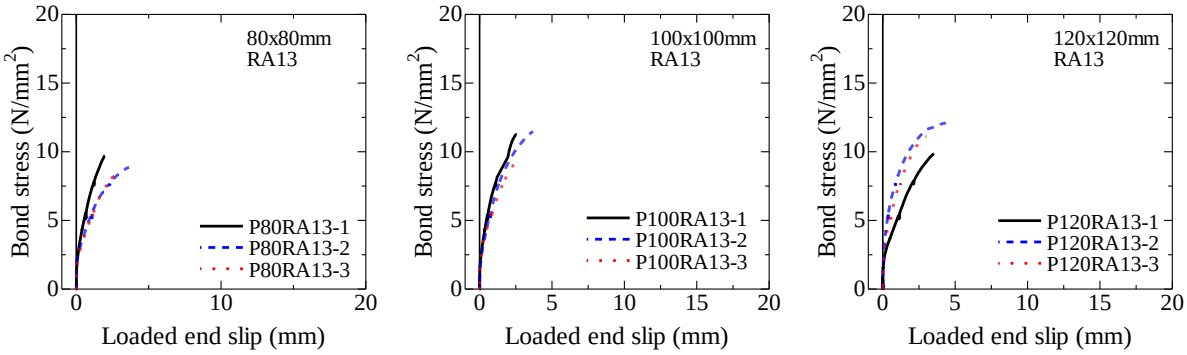

Fig. 2.5 (c) Bond stress – slip relationship (RA13 series)

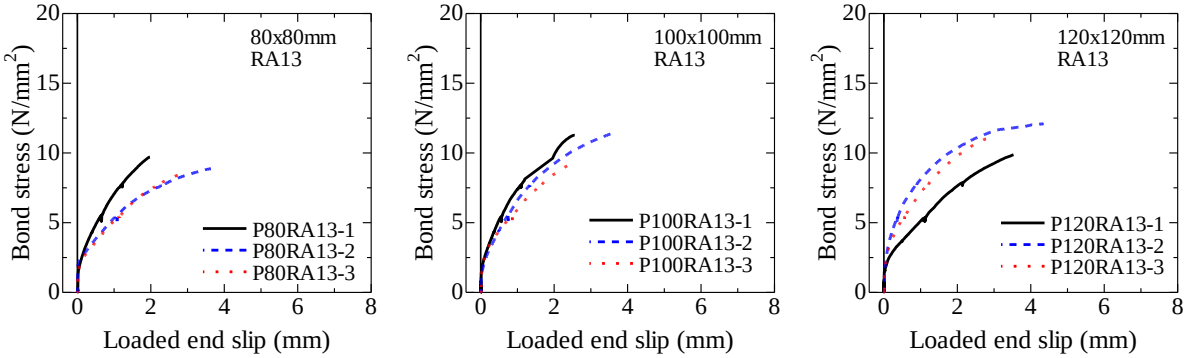

Fig. 2.5 (d) Bond stress – slip relationship (RA13 series, until 8mm)

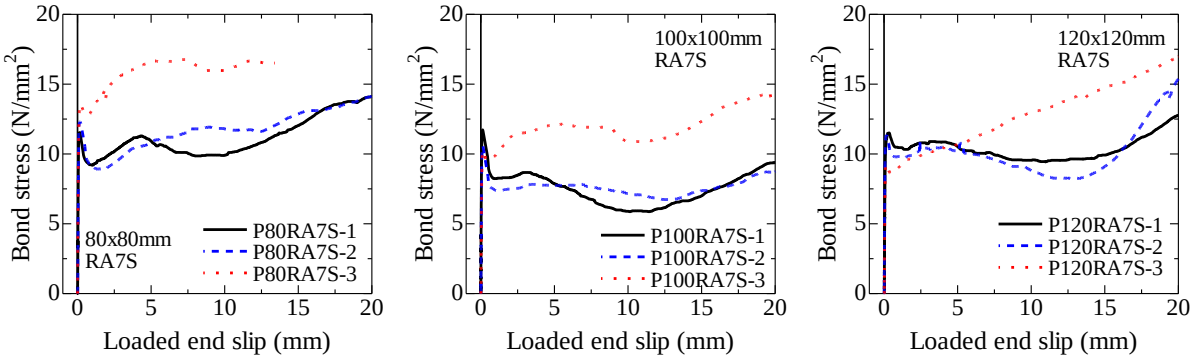

Fig. 2.5 (e) Bond stress – slip relationship (RA7S series)

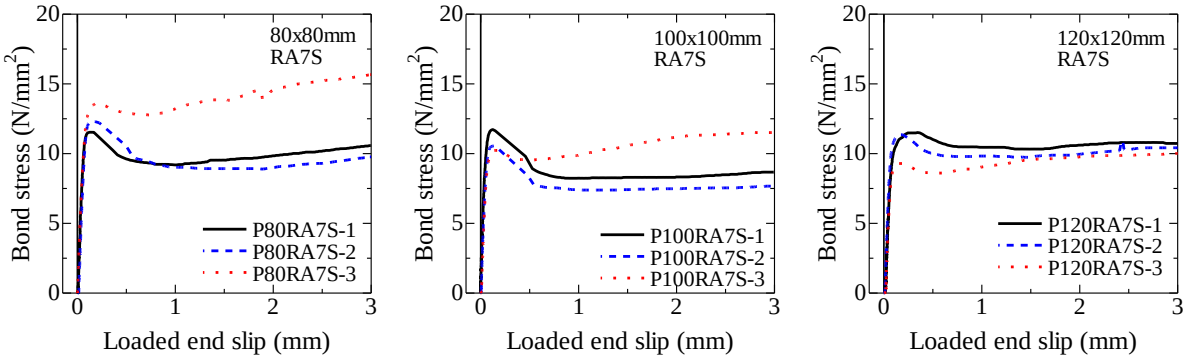

Fig. 2.5 (f) Bond stress – slip relationship (RA7S series, until 3mm)

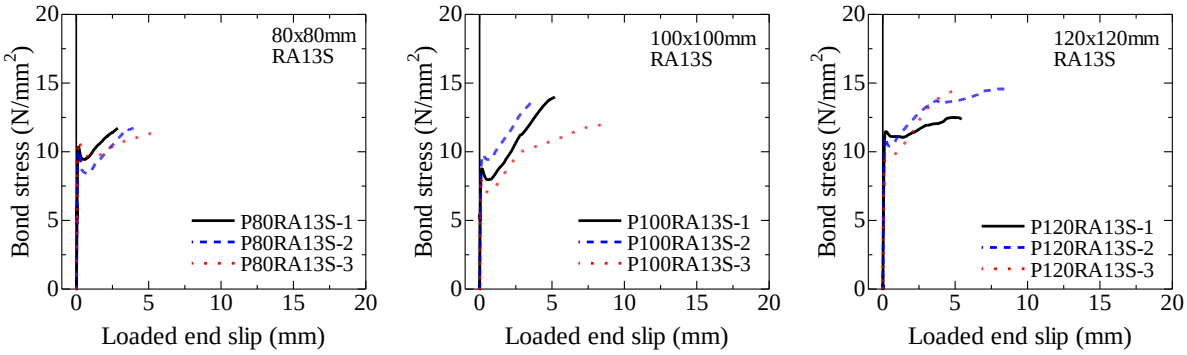

Fig. 2.5 (g) Bond stress – slip relationship (RA13S series)

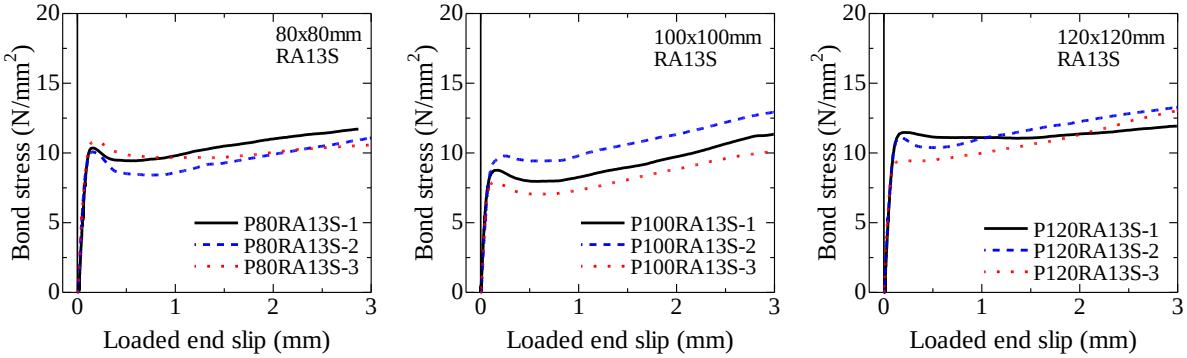

Fig. 2.5 (h) Bond stress – slip relationship (RA13S series, until 3mm)

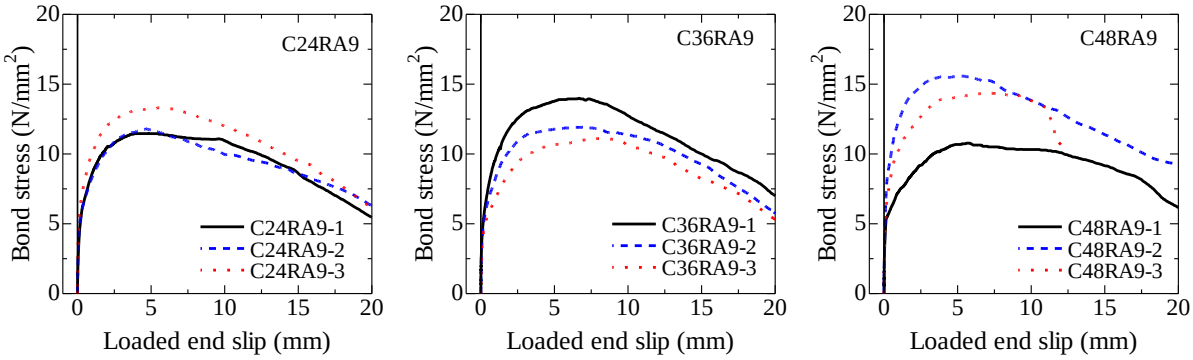

Fig. 2.5 (i) Bond stress – slip relationship (RA9 series)

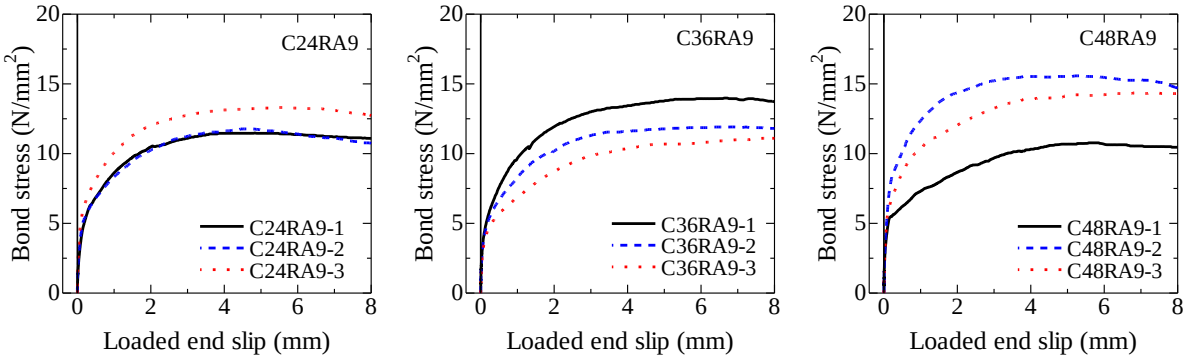

Fig. 2.5 (j) Bond stress – slip relationship (RA9 series, until 8mm)

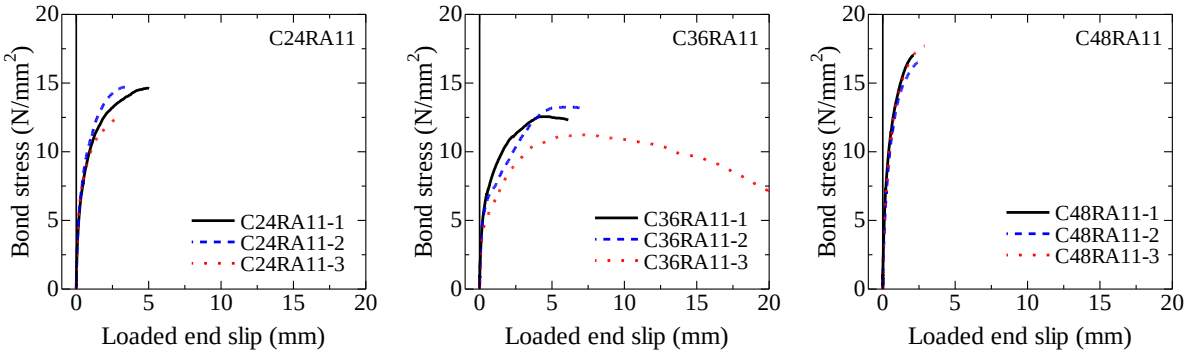

Fig. 2.5 (k) Bond stress – slip relationship (RA11 series)

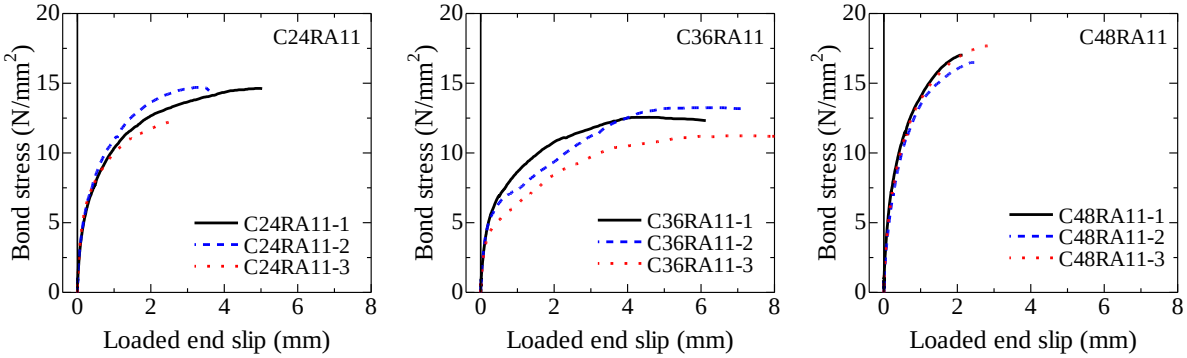

Fig. 2.5 (l) Bond stress – slip relationship (RA11 series, until 8mm)

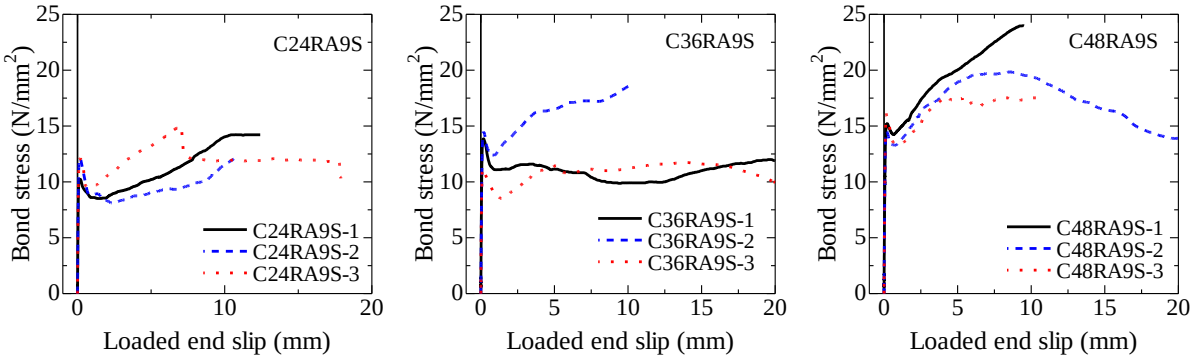

Fig. 2.5 (m) Bond stress – slip relationship (RA9S series)

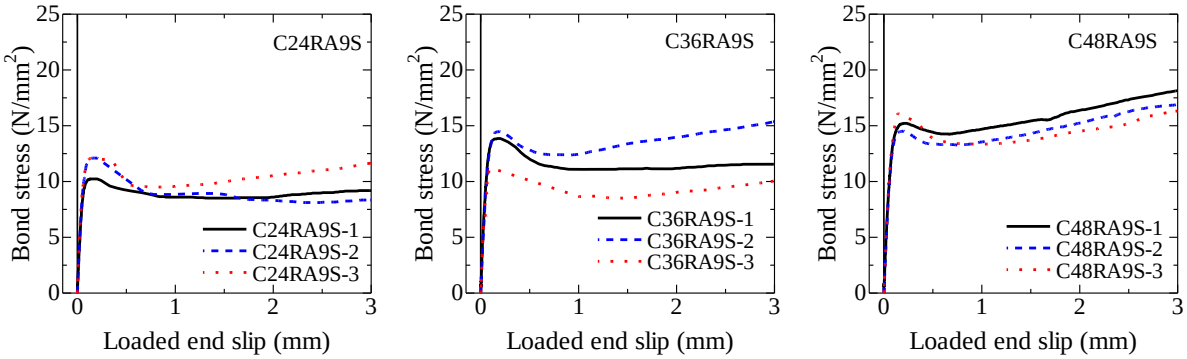

Fig. 2.5 (n) Bond stress – slip relationship (RA9S series, until 3mm)

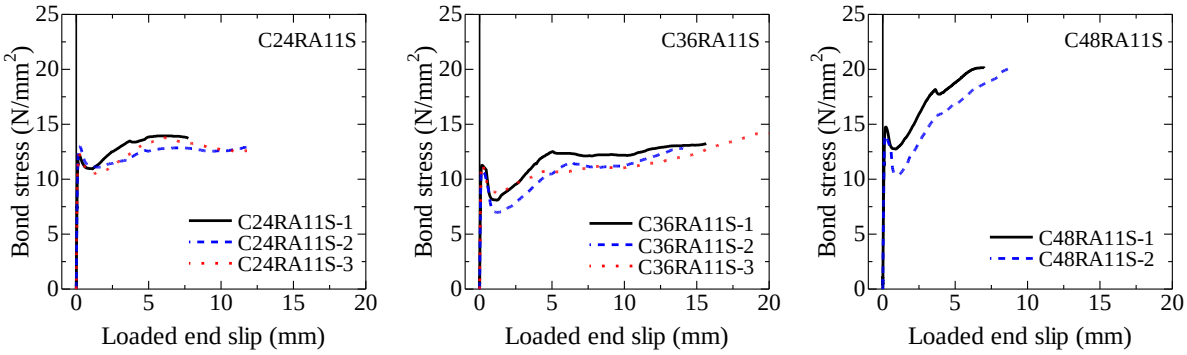

Fig. 2.5 (o) Bond stress – slip relationship (RA11S series)

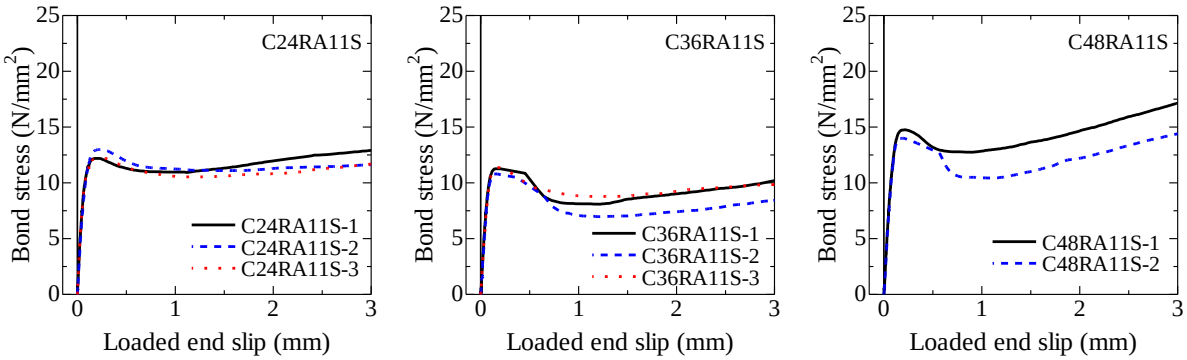

Fig. 2.5 (p) Bond stress – slip relationship (RA11S series, until 3mm)

2.3 Tensile Bond Test

2.3.1 Outline of tensile bond test

The purpose of tensile bond test is to obtain measured crack width to compare with calculated value by the proposing formulas.

Specimen for tensile bond test is shown in Fig. 2.6. The specimen is a concrete prism with length of 1680mm using same reinforcement and same batch of concrete with pullout bond. There are also two series of tensile bond test. The first series with the sectional size of concrete prism varies as 80mm x 80mm, 100mm x100mm and 120mm x120mm. While the second series with the same sectional size of concrete which is 100mm x 100mm but the concrete strength varies as 24MPa, 36MPa and 48MPa. The combination of each parameter is just same as pullout bond test.

Fourteen Pi-gauges which along the axial direction were set on the two sides of concrete surface to measure crack width. The interval of those Pi-gauges is also shown in Fig. 2.6. The experimental crack width is measured by the deformation in one section where corresponding to a couple of LVDTs on symmetrical side of concrete prism. The one crack width is measured for the section until the second crack occurs in same section. Two LVDTs were set beside the specimen to measure the total deformation.

Each Specimen are subjected to tensile load until it reaches to a particular value in order to ensure the crack will take place and not to break the AFRP bar. To make sure crack appears before AFRP bar broken, three slits were conducted in two specimens (120mm x 120mm, reinforced with RA7and RA7S)

before loading as shown in Fig.2.7. The section area at slit is as same as 80mm x 80mm. Fig. 2.8 gives the photo of one prepared specimen for tensile bond test.

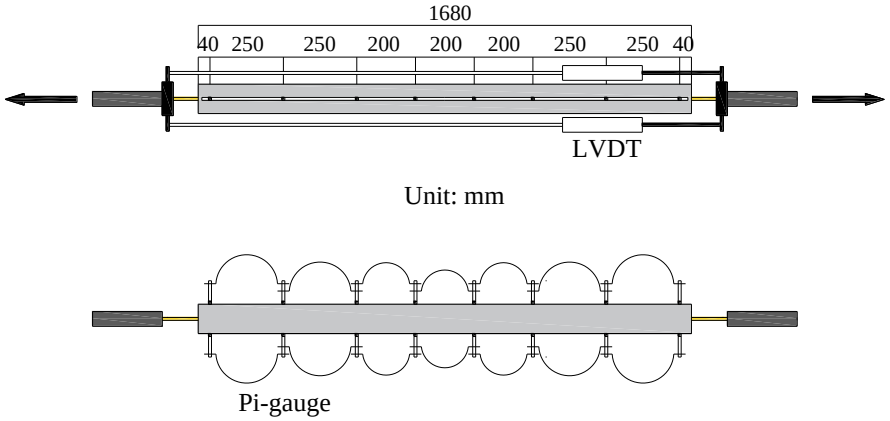

Fig. 2.6 Details and loading method of tensile bond test

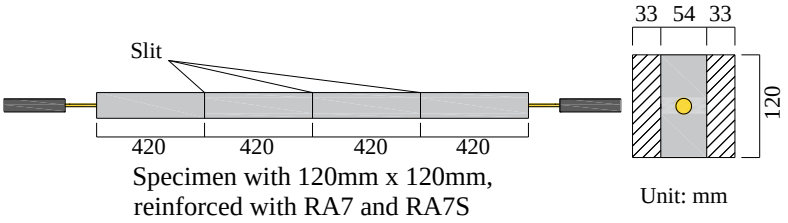

Fig. 2.7 Details for tensile bond specimen of RA7&RA7S series

Fig. 2.8 Photo of one prepared specimen for tensile bond test

Table 2.5 shows the list of specimens for tensile bond test. As mentioned before, the upper limit load was set for safety.

Table 2.5 (a) List of tensile bond test specimen (first series)

Specimen ID	Sectional size (mm x mm)	Reinforcement	Upper limit load (kN)
T-80RA7	80x80	RA7	50
T-100RA7	100x100		35
T-120RA7	120x120		30
T-80RA7S	80x80	RA7S	50*
T-100RA7S	100x100		35
T-120RA7S	120x120		30
T-80RA13	80x80	RA13	100
T-100RA13	100x100		100
T-120RA13	120x120		100
T-80RA13	80x80	RA13S	100
T-100RA13	100x100		100
T-120RA13	120x120		100

*: AFRP bar was broken at 40.2 kN

Table 2.5 (b) List of tensile bond test specimen (second series)

Specimen ID	Concrete strength (N/mm^2)	Reinforcement	Upper limit load (kN)
T-C24RA9	28.5 (C24)	RA9	60
T-C24RA9S		RA9S	60
T-C24RA7		RA11	70
T-C24RA7S		RA11S	70
T-C36RA7S	37.6 (C36)	RA9	60
T-C36RA7S		RA9S	60
T-C36RA13		RA11	70
T-C36RA13		RA11S	70
T-C48RA13	48.5 (C48)	RA9	60
T-C48RA13		RA9S	60
T-C48RA13		RA11	70
T-C48RA13		RA11S	70

2.3.2 Test results of tensile bond test

Final crack patterns after loading are shown in Table 2.6. The perpendicular dashed line shows the location of the fixed points of Pi-gauges. It is obviously that there is a huge difference between the two specimens reinforced with two types of AFRP bar. A good bond performance which means the higher bond stiffness (sand-coated series) can lead larger numbers of cracks. Meanwhile, the first series test results indicate that the crack spacing increases as the sectional size becomes larger. The number of cracks will increasing when the reinforcement ratio decreased. However, the concrete strength does not have a large influence on the crack patterns.

Table 2.6 (a) Crack patterns for specimen reinforced with RA7&RA7S

	RA7	RA7S
80mm x 80mm		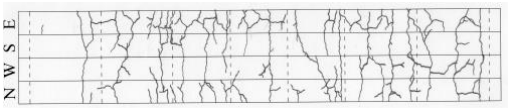
100mm x 100mm	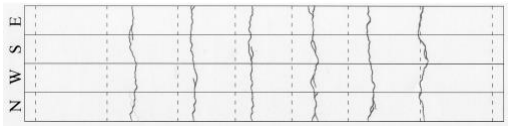	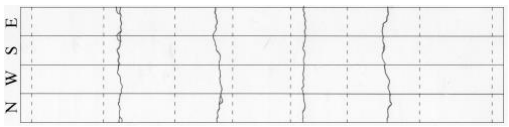
120mm x 120mm	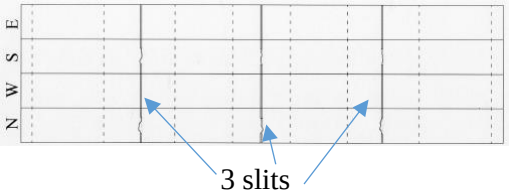	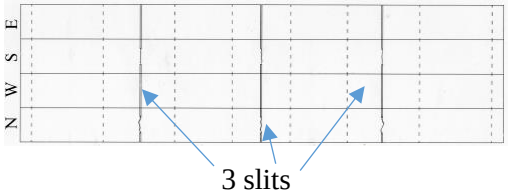

Table 2.6 (b) Crack patterns for specimen reinforced with RA13&RA13S

	RA13	RA13S
80mm x 80mm	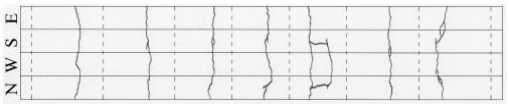	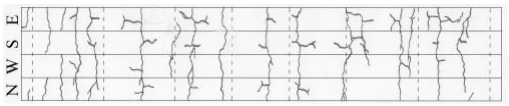
100mm x 100mm	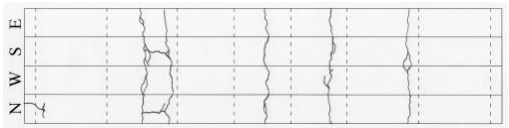	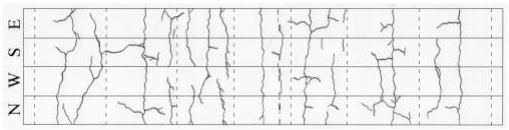
120mm x 120mm	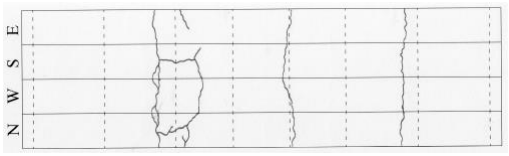	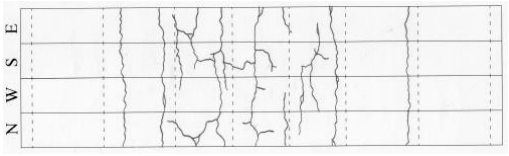

Table 2.6 (c) Crack patterns for specimen reinforced with RA9&RA9S

	RA9	RA9S
C24	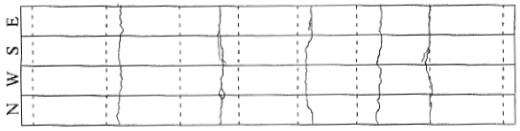	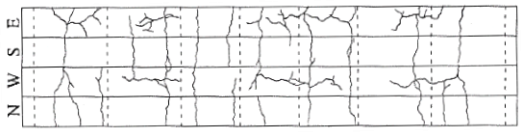
C36	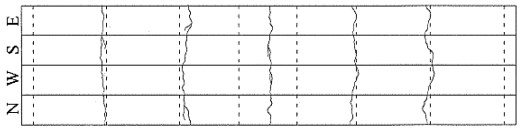	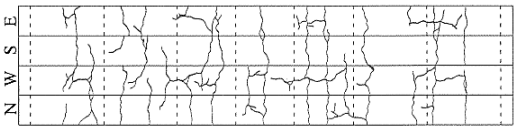
C48	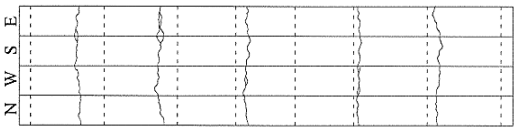	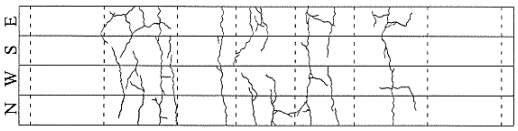

Table 2.6 (d) Crack patterns for specimen reinforced with RA11&RA11S

	RA11	RA11S
C24	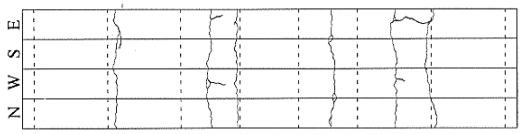	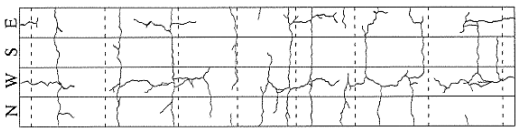
C36	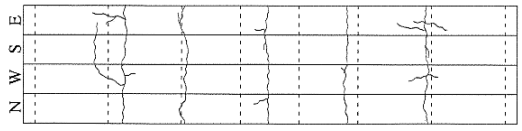	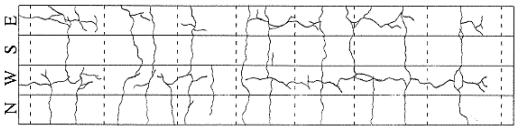
C48	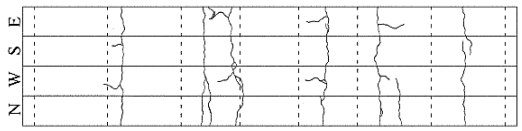	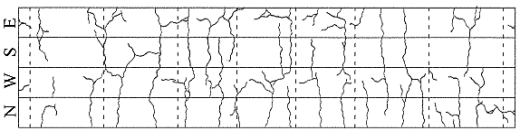

Tensile load versus total deformation curves are shown in Fig. 2.9. The straight lines from the origin indicate the relationship for bare reinforcement. Tension stiffening effect can be found in all the specimens. With the sectional size of concrete increasing, the effect will become higher. However, the increasing of concrete strength does not provide a much higher tension stiffening effect. The curves show several drops of tensile load at which a new crack takes place.

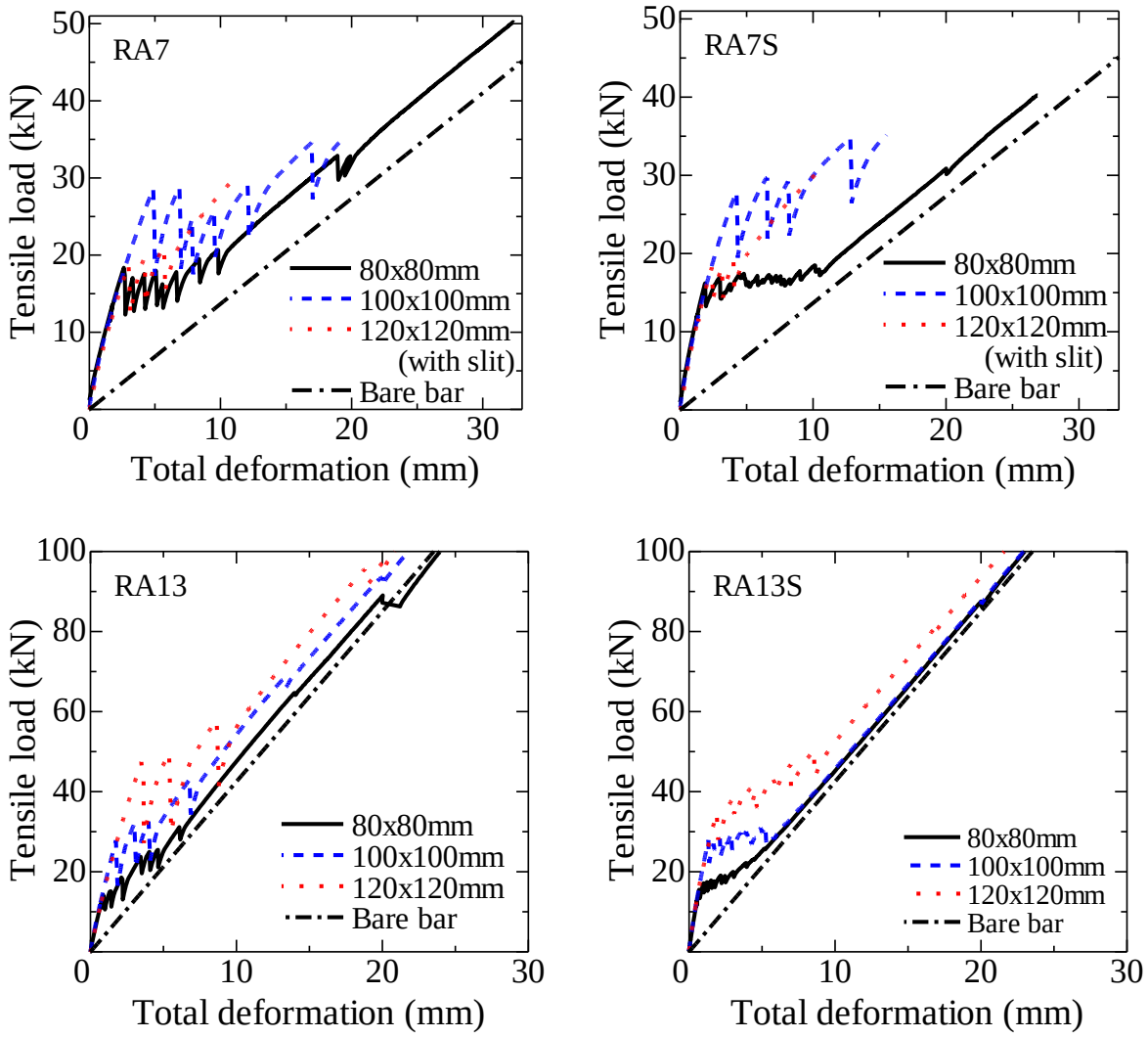

Fig. 2.9 (a) Tensile load-total deformation relation for first series

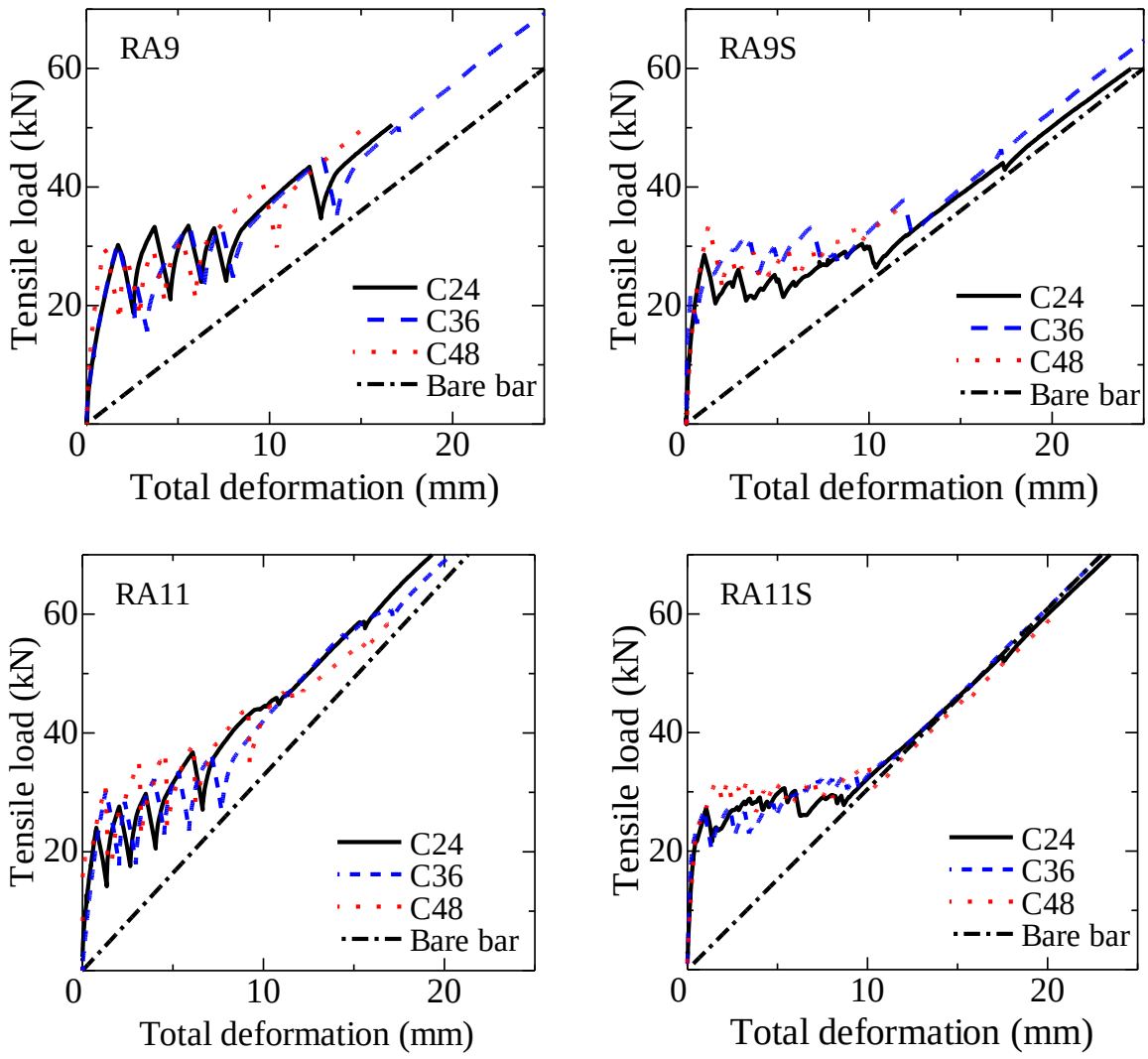

Fig. 2.9 (b) Tensile load - total deformation relation for second series

CHAPTER 3

Tri-Linear Model for Bond Constitutive Law

3.1 Definition of Tri-Linear Model

As there is a large difference between the bond behaviors of two types of AFRP bar, two types of tri-linear model are introduced. One is for the non-coated type and the other is for sand-coated type.

3.1.1 Tri-linear model for non-coated type AFRP bar

Fig. 3.1 shows the tri-linear model for non-coated type AFRP bar.

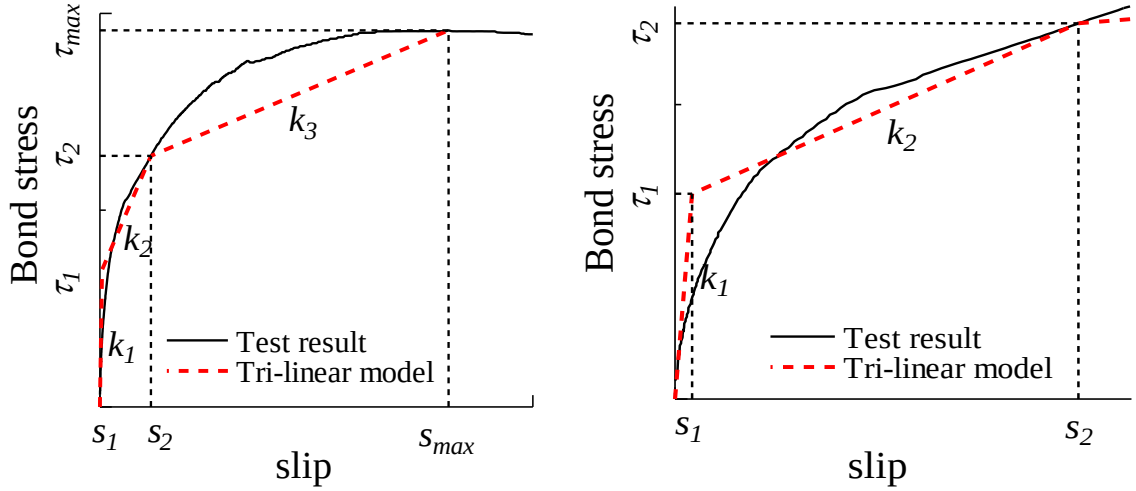

Extended image for the part of k_1 and k_2

Fig. 3.1 Definition of tri-linear model for non-coated type bar

The tri-linear model for non-coated type only consider the increase branch of the bond stress because the s_{max} is large enough that can provide a widely range crack width prediction formulas. The definition and mathematical expressions are given as follows.

$$\tau_{\max} = \text{maximum bond stress}$$

$$s_{\max} = \text{slip at } \tau_{\max}$$

$$\tau_2 = \frac{2}{3}\tau_{\max}$$

$$s_2 = \text{slip at } \tau_2$$

$$\tau_1 = k_1 \cdot s_1$$

$$s_1 = \frac{6 \cdot G_{f2} - 2 \cdot s_2 \cdot \tau_{\max}}{3 \cdot k_1 \cdot s_2 - 2 \cdot \tau_{\max}}$$

G_{f2} = fracture energy during bond stress from 0 to τ_2

From the Fig. 3.1, the two straight line of k_1 and k_2 cut the curve of test result into two enclosed parts. The s_1 can be calculated by leading those two parts with same area. The τ_{max}, s_{max}, s_2, G_{f2} and k_1 can be directly obtained from pullout bond test.
Therefore, the bond stiffness of each part can be described as:

$$k_1 = \text{initial stiffness},\ k_2 = \frac{\tau_2 - \tau_1}{s_2 - s_1}, k_3 = \frac{\tau_{\max} - \tau_2}{s_{\max} - s_2}$$

3.1.2 Tri-linear model for sand-coated type AFRP bar

Fig. 3.2 shows the tri-linear model for sand-coated type AFRP bar.

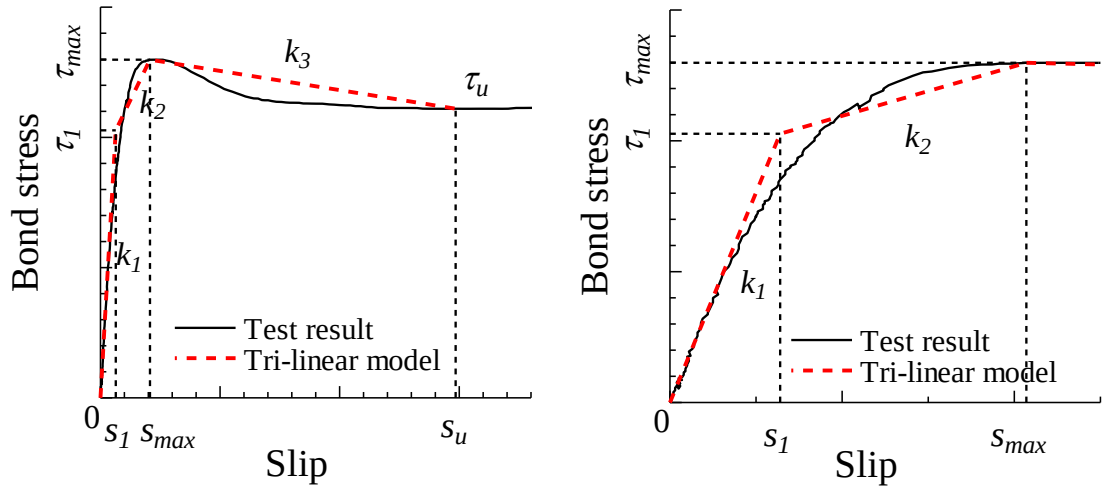

Fig. 3.2 Definition of tri-linear model for sand-coated type bar

Unlike the non-coated type, those sand-coated types bar provide a much higher initial stiffness. A high bond stress with too little slippage from the experiments cannot give enough information for modeling bond constitutive law. Meanwhile, bond stress of all the sand-coated types specimens show a remarkable drop after reaching the slipping bond stress. In addition, after the bond reduction, the bond stress soon increases again. Therefore, τ_u which means the minimum value after slipping bond stress is considered as a characteristic value.

The definition and mathematical expressions are given as follows.

τ_u = minimum bond stress after slipping bond stress

s_u = slip at τ_u

$\tau_{\max}$ = slipping bond stress

$s_{\max}$ = slip at $\tau_{\max}$

$\tau_1 = k_1 \cdot s_1$

$$s_1 = \frac{2 \cdot G_{f2} - s_{\max} \cdot \tau_{\max}}{k_1 \cdot s_{\max} - \tau_{\max}}$$

G_{f2} = fracture energy during bond stress from 0 to τ_2

The calculation method of s_1 is same as the non-coated type.
The bond stiffness can be presented as:

$$k_1 = \text{initial stiffness}, \quad k_2 = \frac{\tau_{\max} - \tau_1}{s_{\max} - s_1}, k_3 = \frac{\tau_u - \tau_{\max}}{s_u - s_{\max}}$$

3.2 Theoretical Calculation Formulas

Based on each bond stiffness which presented in chapter 3.1.1 and 3.1.2, a simple form linear function of bond constitutive law can be obtained. They are:

Non-coated type

$\tau_1 = k_1 \cdot s$ $\quad (s \le s_1)$

$\tau_2 = k_2 \cdot (s - s_1) + \tau_1$ $\quad (s_1 < s \le s_2)$

$\tau_{\max} = k_3 \cdot (s - s_2) + \tau_2$ $\quad (s > s_2)$

Sand-coated type

$\tau_1 = k_1 \cdot s$ $\quad (s \le s_1)$

$\tau_{\max} = k_2 \cdot (s - s_1) + \tau_1$ $\quad (s_1 < s \le s_2)$

$\tau_u = k_3 \cdot (s - s_{\max}) + \tau_{\max}$ $\quad (s > s_{\max})$

In fact, there is no difference between the mathematical calculation processes of two types of tri-linear model except the symbols. Therefore, Eq. (3.1) ~ Eq. (3.4) can be used for both type. However, when calculating the k_3, it requires for s_2 and τ_2 which is corresponding to the τ_{max} and s_{max} in sand-coated type, replacing s_2 and τ_2 by τ_{max} and s_{max} in Eq. (3.5) ~ Eq. (3.7) can obtain the calculation formulas for sand-coated type which presented by Eq. (3.8) ~ Eq. (3.10).

The Eq. (1) can be solved by using the linear function of τ and s. And with an assumption that the slip at loaded end gives a half of crack width, theoretical calculation formulas for crack width Eq. (3.1) ~ Eq. (3.10) can be obtained.

Eq. (3.1) presents the calculation by k_1 which means the initial stiffness.

$$w_{cr} = 2 \cdot \sqrt{\frac{2\sigma_{ct} A_c}{k_1 \phi_b} \left(\varepsilon_l - \frac{1+np}{2} \cdot \frac{\sigma_{ct} A_c}{E_b A_b} \right)} \qquad \left(w_{cr} < 2 \cdot s_1 \right) \tag{3.1}$$

Eq. (3.2) ~ Eq. (3.4) are calculated by k_2. After reaching to τ_1, the bond stress moves to second branch till the τ_2. The k_2 can vary positive, negative or just equal to zero. So the formulas are divide into 3 conditions depended on the valve of k_2.

$$w_{cr} = 2 \cdot \left\{ (1 - \frac{k_1}{k_2}) \cdot s_1 + \sqrt{\frac{2\sigma_{ct} A_c}{k_2 \phi_b} \left(\varepsilon_l - \frac{1+np}{2} \cdot \frac{\sigma_{ct} A_c}{E_b A_b} \right) + {s_1}^2 \cdot \frac{k_1 \cdot (k_1 - k_2)}{{k_2}^2}} \right\} \tag{3.2}$$

$$\left(k_2 > 0, 2 \cdot s_1 < w_{cr} < 2 \cdot s_2 \right)$$

$$w_{cr} = 2 \cdot \left\{ (1 - \frac{k_1}{k_2}) \cdot s_1 - \sqrt{\frac{2\sigma_{ct} A_c}{k_2 \phi_b} \left(\varepsilon_l - \frac{1+np}{2} \cdot \frac{\sigma_{ct} A_c}{E_b A_b} \right) + {s_1}^2 \cdot \frac{k_1 \cdot (k_1 - k_2)}{{k_2}^2}} \right\} \tag{3.3}$$

$$\left(k_2 < 0, 2 \cdot s_1 < w_{cr} < 2 \cdot s_2 \right)$$

$$w_{cr} = 2 \cdot \left\{ \frac{1}{2} \cdot s_1 + \frac{\sigma_{ct} A_c}{k_1 \phi_b s_1} \left(\varepsilon_l - \frac{1+np}{2} \cdot \frac{\sigma_{ct} A_c}{E_b A_b} \right) \right\} \tag{3.4}$$

$$\left(k_2 = 0, 2 \cdot s_1 < w_{cr} < 2 \cdot s_2 \right)$$

Eq. (3.5) ~ Eq. (3.10) are calculated by k_3. Similar with the k_2, the formulas calculated by k_3 are also have 3 conditions.

$$w_{cr} = 2 \cdot \left\{ s_2 - \frac{\tau_2}{k_3} + \sqrt{\frac{2\sigma_{ct} A_c}{k_3 \phi_b} \left(\varepsilon_l - \frac{1+np}{2} \cdot \frac{\sigma_{ct} A_c}{E_b A_b} \right) + \frac{{\tau_2}^2}{{k_3}^2} - \frac{k_1 s_1 s_2 + \tau_2 s_2 - \tau_2 s_1}{k_3}} \right\} \tag{3.5}$$

$$\left(k_3 > 0, 2 \cdot s_2 < w_{cr} < 2 \cdot s_{\max} \right)$$

$$w_{cr} = 2 \cdot \left\{ s_2 - \frac{\tau_2}{k_3} - \sqrt{\frac{2\sigma_{ct} A_c}{k_3 \phi_b} \left(\varepsilon_l - \frac{1+np}{2} \cdot \frac{\sigma_{ct} A_c}{E_b A_b} \right) + \frac{{\tau_2}^2}{{k_3}^2} - \frac{k_1 s_1 s_2 + \tau_2 s_2 - \tau_2 s_1}{k_3}} \right\} \tag{3.6}$$

$$\left(k_3 < 0, 2 \cdot s_2 < w_{cr} < 2 \cdot s_{\max} \right)$$

$$w_{cr} = 2 \cdot \left\{ \frac{1}{2} \cdot s_1 \cdot \left(1 - \frac{k_1 s_2}{\tau_2} \right) + \frac{1}{2} \cdot s_2 + \frac{\sigma_{ct} A_c}{\phi_b \tau_2} \left(\varepsilon_l - \frac{1+np}{2} \cdot \frac{\sigma_{ct} A_c}{E_b A_b} \right) \right\} \tag{3.7}$$

$$\left(k_3 = 0, 2 \cdot s_2 < w_{cr} < 2 \cdot s_{\max} \right)$$

$$w_{cr} = 2 \cdot \left\{ s_{\max} - \frac{\tau_{\max}}{k_3} + \sqrt{\frac{2\sigma_{ct} A_c}{k_3 \phi_b} \left(\varepsilon_l - \frac{1+np}{2} \cdot \frac{\sigma_{ct} A_c}{E_b A_b} \right) + \frac{\tau_{\max}{}^2}{k_3{}^2} - \frac{k_1 s_1 s_{\max} + \tau_{\max} s_{\max} - \tau_{\max} s_1}{k_3}} \right\} \tag{3.8}$$

$$\left(k_3 > 0, 2 \cdot s_{\max} < w_{cr} < 2 \cdot s_u \right)$$

$$w_{cr} = 2 \cdot \left\{ s_{\max} - \frac{\tau_{\max}}{k_3} - \sqrt{\frac{2\sigma_{ct} A_c}{k_3 \phi_b} \left(\varepsilon_l - \frac{1+np}{2} \cdot \frac{\sigma_{ct} A_c}{E_b A_b} \right) + \frac{\tau_{\max}{}^2}{k_3{}^2} - \frac{k_1 s_1 s_{\max} + \tau_{\max} s_{\max} - \tau_{\max} s_1}{k_3}} \right\} \tag{3.9}$$

$$\left(k_3 < 0, 2 \cdot s_{\max} < w_{cr} < 2 \cdot s_u \right)$$

$$w_{cr} = 2 \cdot \left\{ \frac{1}{2} \cdot s_1 \cdot \left(1 - \frac{k_1 s_{\max}}{\tau_{\max}} \right) + \frac{1}{2} \cdot s_{\max} + \frac{\sigma_{ct} A_c}{\phi_b \tau_{\max}} \left(\varepsilon_l - \frac{1+np}{2} \cdot \frac{\sigma_{ct} A_c}{E_b A_b} \right) \right\} \tag{3.10}$$

$$\left(k_3 = 0, 2 \cdot s_{\max} < w_{cr} < 2 \cdot s_u \right)$$

CHAPTER 4

Parameter Estimation for Theoretical Formulas

The characteristic values of theoretical formulas in Section 3.2 are totally based on the test results of pullout bond test. Thus cannot be widely use of practical application. The bond stiffness is considered as the key to the formulas. An estimation of the bond stiffness should be conducted. On the other hand, bond stiffness is determined by bond stress and slip which can easily considered that the concrete compressive strength (f_c) and bar diameter (d_b) are the main effective factors.

The estimation is based on all the test results of pullout bond test which includes two series experiment with different bar diameter and concrete strength. However, regarding to the first series experiment, it is only considered the results of specimens with sectional size of 100x100mm, considering the sectional size of concrete does not have a large influence on the bond behavior.

4.1 Parameter Estimation for Non-Coated Type Specimen

This chapter aims to directly figure out the main effective parameters which influence the bond stiffness (k_1, k_2 and k_3) and some other characteristic values such as τ_{max} and s_{max} by the regression analysis of the test results of pullout bond test.

The max. bond stress plays an important role in determining the proposed tri-linear model. Fig. 4.1 shows the relationship between max. bond stress (slipping bond stress for sand-coated type) and concrete strength for both two types including the specimens failure by concrete splitting. It can be found that regardless of the surface treatment, the max. bond stress of both two types show the similar value and tendency. Moreover, Fig. 4.2 shows the relationship between the max. bond stress of two types which also includes the specimens failed by concrete splitting. It is feasible to estimate the max. bond stress for both types at same time because they are almost the same if under the same combination of bar diameter and concrete strength.

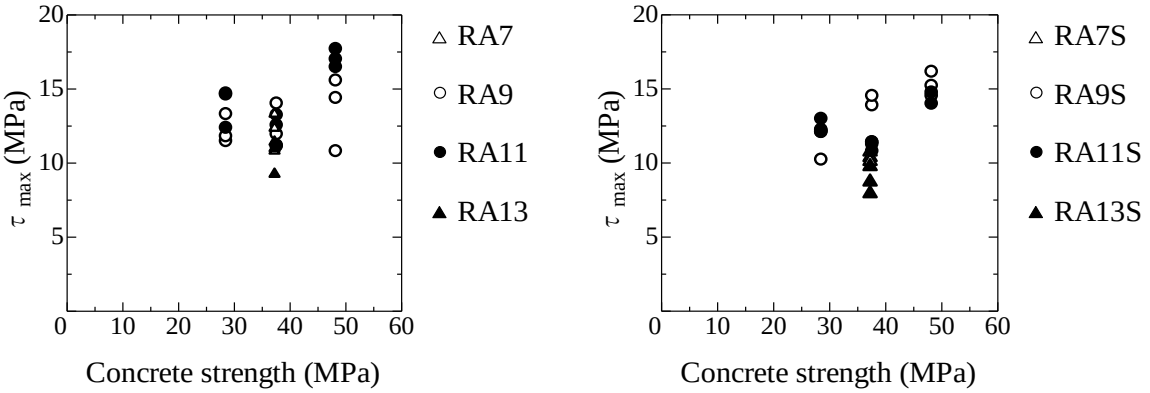

Fig. 4.1 Max. bond stress – concrete strength relation

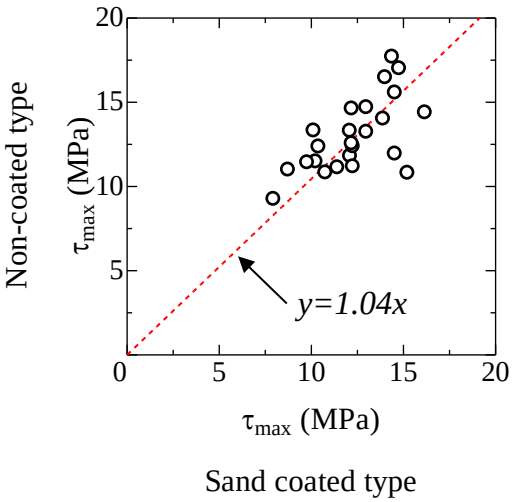

Fig. 4.2 Relationship between the max. bond stress of two types

Fig. 4.3 shows the relationship between concrete strength and max. bond stress including both types. The fitting line is considered as a function of $f_c^{1/3}$. In addition, to investigate the influence of bar diameter on the max. bond stress, Fig. 4.4 shows the relationship between bar diameter and normalized max. bond stress. There is no clear relationship between max. bond stress and bar diameter. Therefore, the max. bond stress is only expressed by a function of concrete strength.

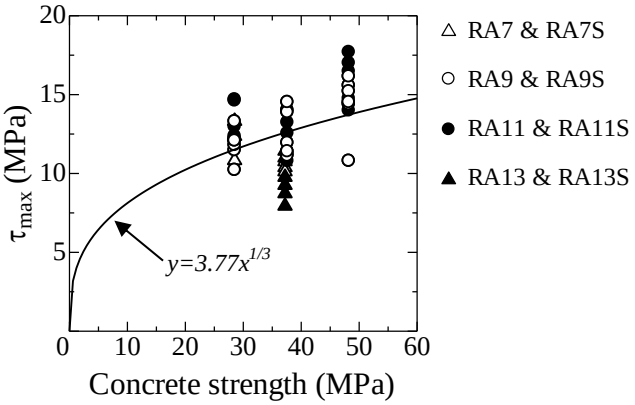

Fig. 4.3 $\tau_{max} - f_c$ relation

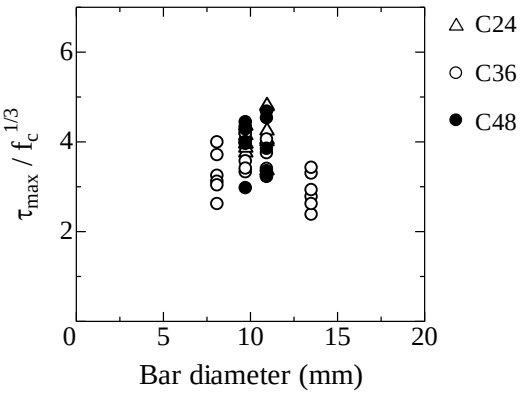

Fig. 4.4 Normalized $\tau_{max} - d_b$ relation

$$\tau_{\max} = 3.77 f_c^{1/3} \tag{4.1}$$

To determine the value of k_1, τ_1 and s_1 are discussed. Fig. 4.5 shows the relationship between τ_1 and concrete strength. It can be found that concrete strength does not influence the τ_1. There is a tendency, as shown in Fig. 4.6, that is the τ_1 is in inverse proportion to the bar diameter. Fig. 4.7 and Fig. 4.8 show the relationships between s_1 and bar diameter and concrete strength, respectively. There is no definite relationship between them, therefore it is considered as a constant value (0.035mm) which is equal to the average value from the experiment.

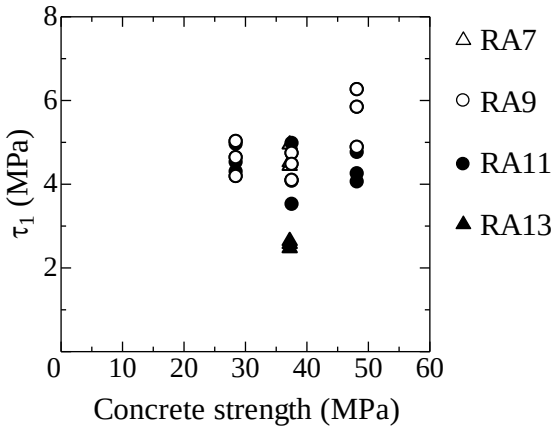

Fig. 4.5 τ_1 - f_c relation
(Non-coated type)

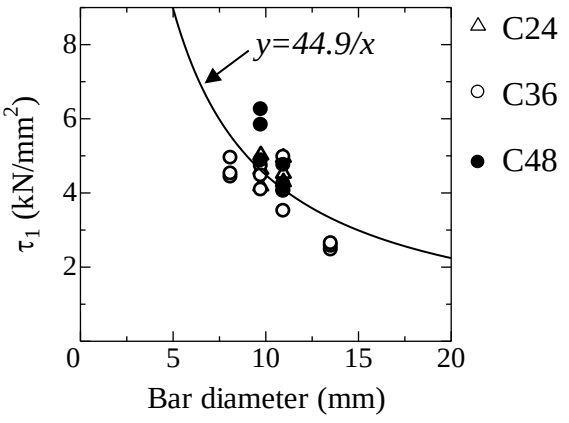

Fig. 4.6 τ_1 - d_b relation
(Non-coated type)

$$\tau_1 = \frac{44.9}{d_b} \tag{4.2}$$

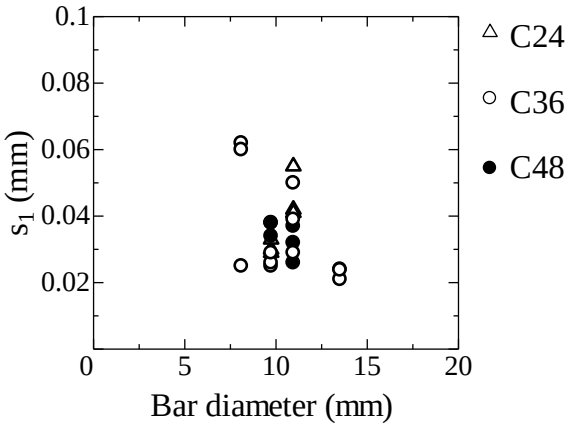

Fig. 4.7 s_1 - d_b relation
(Non-coated type)

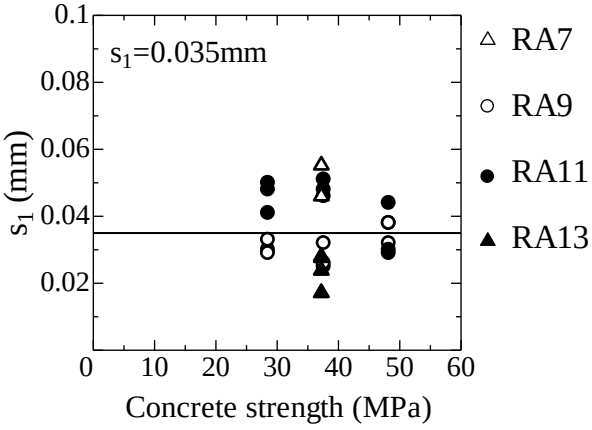

Fig. 4.8 s_1 – f_c relation
(Non-coated type)

$$s_1 = 0.035\text{mm} \tag{4.3}$$

$$k_1 = \frac{\tau_1}{s_1} = \frac{1.28\times10^3}{d_b} \tag{4.4}$$

Fig. 4.9 shows the relationship between concrete strength and k_2 including all the specimens. Basically, as s_1 is considered as a constant value and τ_1 does not change too much, the τ_2 (determined by τ_{max}) and its corresponding slip s_2 dominate the value of k_2. However, those specimens failed by concrete splitting do not give the true value of τ_{max}, that cause the k_2 unreal for those specimens. The relationship between concrete strength and k_2 for the specimens only failed by pullout is shown in Fig. 4.10. Although it shows some variations, the concrete strength is slightly effect the value of k_2. Therefore, k_2 is proposed as the function of $f_c^{1/3}$.

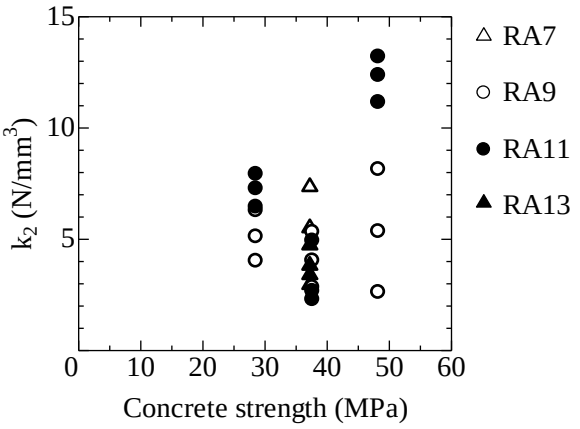

Fig. 4.9 k_2 - f_c relation
(Non-coated type)

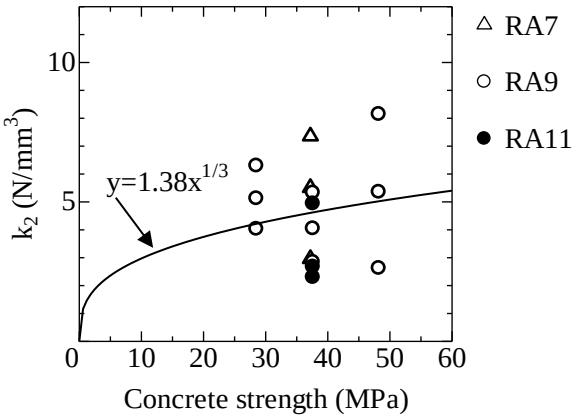

Fig. 4.10 k_2 - f_c relation
(Non-coated type, specimen failed by pullout)

$$k_2 = 1.38 f_c^{1/3} \tag{4.5}$$

Regarding to the k_3, it is similar to the situation of k_2. As shown in Fig. 4.11, specimen failed by concrete splitting usually give a high bond stress while little slippage that may lead a much higher k_3. The relationship between concrete strength and k_3 for those specimens failed by pullout is shown in Fig. 4.12. On the other hand, the k_3 is determined by τ_{max}, τ_2, s_{max} and s_2 where the most important parameter is s_{max}. It is attribute to that when the bond stress is near the τ_{max} the curve becomes moderate with a slightly increasing of bond stress but a relatively large slip. Fig. 4.13 shows the relationship between s_{max} and k_3. As expected, the k_3 is in inverse proportion to the s_{max}.

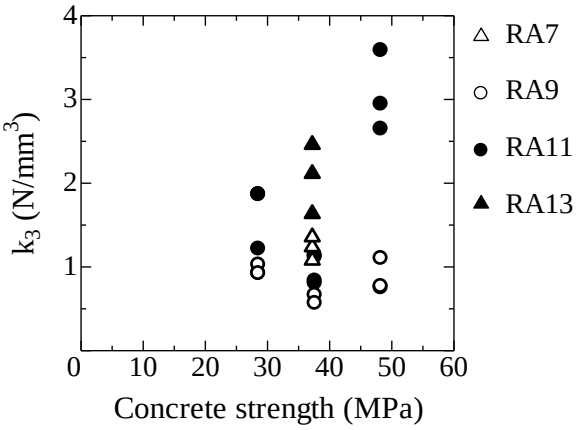

Fig. 4.11 k_3 - f_c relation
(Non-coated type)

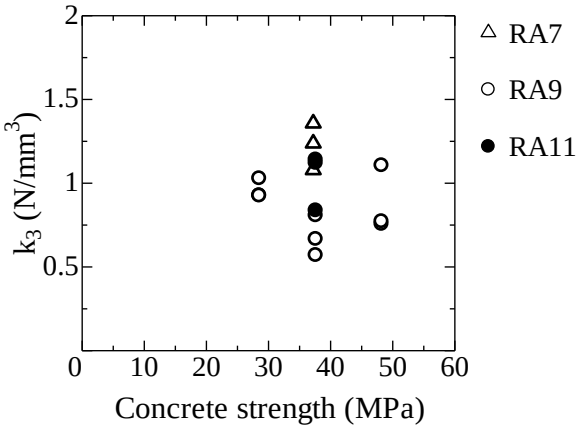

Fig. 4.12 k_3 - f_c relation
(Non-coated type, specimen failed by pullout)

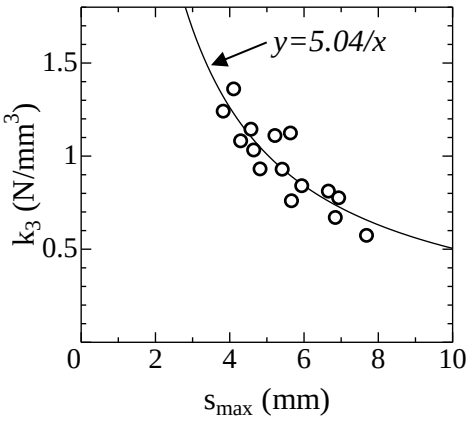

Fig. 4.13 $k_3 - s_{max}$ relation
(Non-coated type)

$$k_3 = \frac{5.04}{s_{\max}} \tag{4.6}$$

Fig. 4.14 shows the relationship between bar diameter and $s_{max.}$ As the bar diameter increasing, the s_{max} also increases. The relationship between concrete strength and the normalized s_{max} by divide bar diameter is shown in Fig. 4.15.

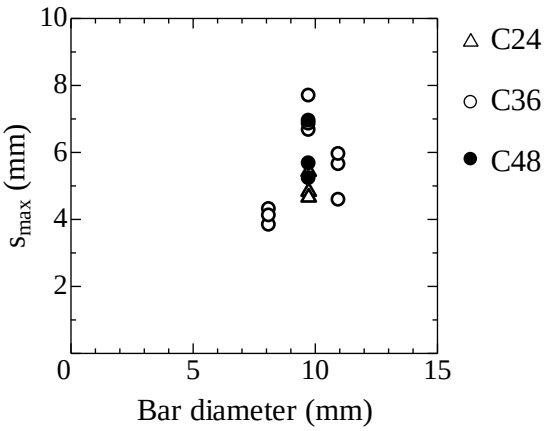

Fig. 4.14 s_{max} - d_b relation
(Non-coated type)

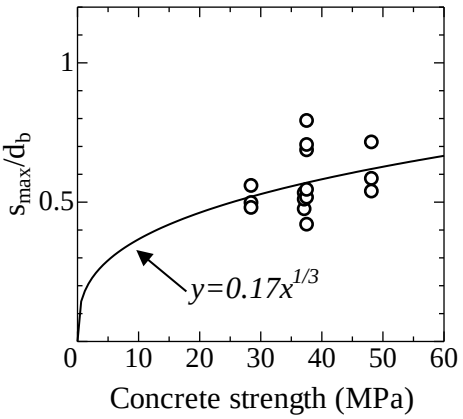

Fig. 4.15 normalized s_{max} - f_c relation
(Non-coated type)

$$s_{\max} = 0.17 f_c^{1/3} d_b \tag{4.7}$$

$$k_3 = \frac{5.04}{s_{\max}} = \frac{29.6}{d_b f_c^{1/3}} \tag{4.8}$$

4.2 Parameter Estimation for Sand-Coated Type Specimen

Under the definition of tri-linear model for sand-coated type, the max. bond stress (defined as slipping bond stress in pullout bond test) has more effective in influencing the bond stiffness than the non-coated type ones.

Unlike the non-coated type specimens, the sand-coated surface can lead a large initial stiffness and it is mainly influenced by the bar diameter. Fig. 4.16 shows a clear relationship which the initial stiffness is in inverse proportion to the bar diameter. The large influence of concrete strength cannot be recognized from Fig. 4.17.

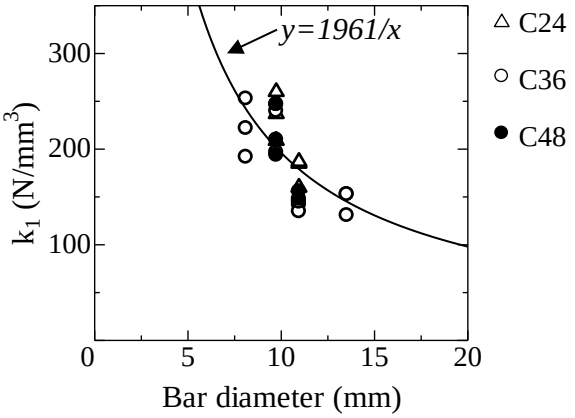

Fig. 4.16 k_1 - d_b relation
(Sand-coated type)

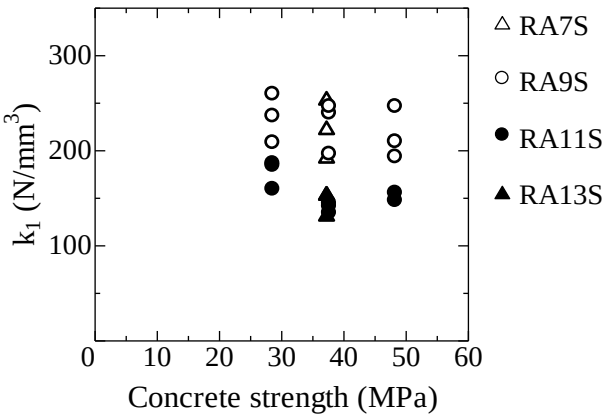

Fig. 4.17 $k_1 - f_c$ relation
(Sand-coated type)

$$k_1 = \frac{1.96\times10^3}{d_b} \tag{4.9}$$

Fig. 4.18 shows the relationship between the concrete strength and the ratio of τ_1 to τ_{max}. Regardless of the concrete strength the ratio shows an ideal result which is that τ_1 is 0.83 times $\tau_{max.}$ Moreover, Fig. 4.19 also indicates that the τ_u which is the minimum value after max. bond stress (slipping bond stress) is 0.82 times $\tau_{max.}$.The bond stiffness can be calculated when the value of slip is determined.

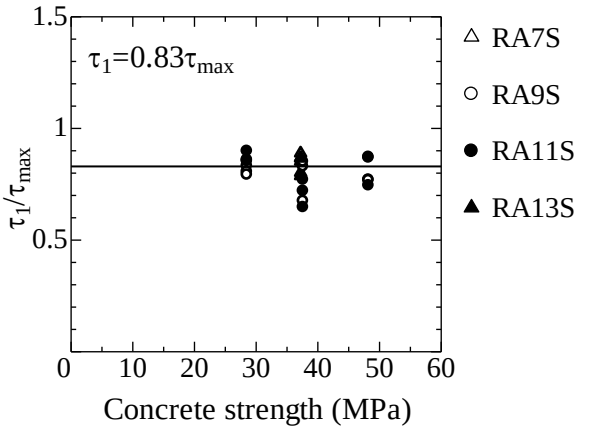

Fig. 4.18 τ_1 / τ_{max} - f_c relation
(Sand-coated type)

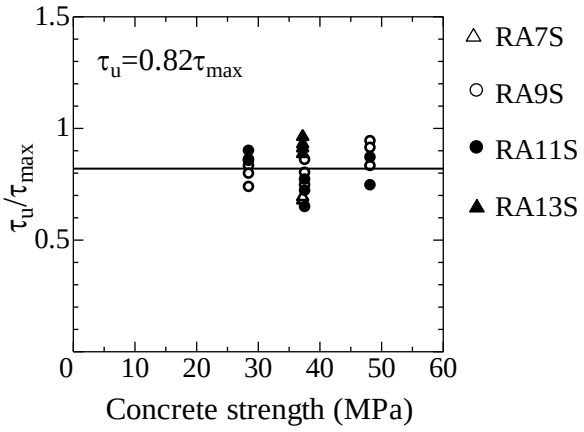

Fig. 4.19 τ_u / τ_{max} - f_c relation
(Sand-coated type)

$$s_1 = \frac{\tau_1}{k_1} = \frac{0.83\tau_{\max}}{k_1} = 0.0016 f_c^{1/3} d_b \tag{4.10}$$

Regarding to the $s_{max,}$ as showing in Fig. 4.20 and Fig. 4.21, no significant influence of the concrete strength or bar diameter on s_{max} is found. The s_{max} is considered as a constant value which is equal to the average value from test results.

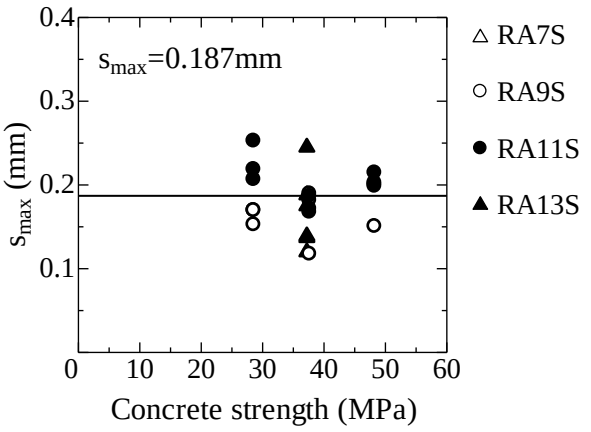

Fig. 4.20 s_{max} - f_c relation
(Sand-coated type)

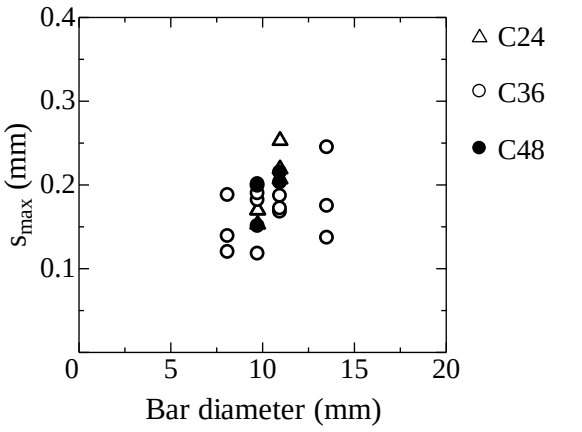

Fig. 4.21 s_{max} – d_b relation
(Sand-coated type)

$$s_{\max} = 0.187\text{mm} \tag{4.11}$$

$$k_2 = \frac{\tau_{\max} - \tau_1}{s_{\max} - s_1} = \frac{0.64 f_c^{1/3}}{0.187 - 0.0016 f_c^{1/3} d_b} \tag{4.12}$$

Relationship between concrete strength and s_u is shown in Fig. 4.22. As concrete strength increases, the s_u becomes smaller. The RA13S specimens show a relatively large drop comparing with other diameter

ones. However the bar diameter can hardly influence on the s_u as shown in Fig. 4.23.

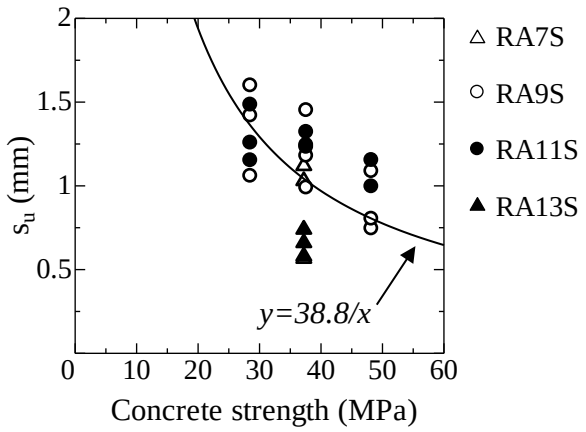

Fig. 4.22 s_u - f_c relation
(Sand-coated type)

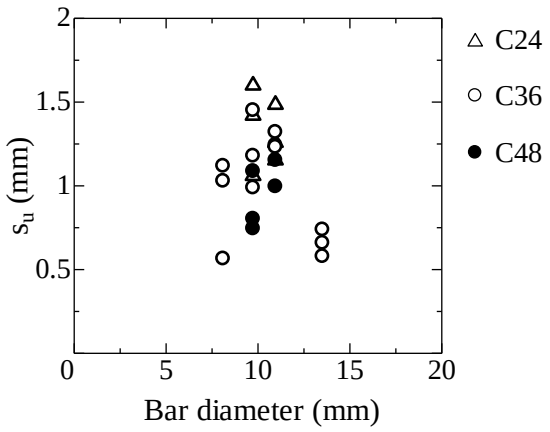

Fig. 4.23 s_u – d_b relation
(Sand-coated type)

$$s_u = \frac{38.8}{f_c} \tag{4.13}$$

$$k_3 = \frac{\tau_u - \tau_{\max}}{s_u - s_{\max}} = \frac{0.68 f_c^{1/3}}{38.8 f_c^{-1} - 0.187} \tag{4.14}$$

4.3 Expression of Tri-Linear Model

Summarizing the estimated parameters in last two sections, the tri-linear model can be expressed and the expression is shown in Table 4.1.

Table. 4.1 Expression of tri-linear model

Non-coated type		Sand-coated type	
Parameter	Expression	Parameter	Expression
τ_1	$\frac{44.9}{f_c}$	τ_1	$3.13 f_c^{1/3}$
s_1	0.035mm	s_1	$0.0016 f_c^{1/3} d_b$
τ_2	$2.51 f_c^{1/3}$	τ_{max}	$3.77 f_c^{1/3}$
s_2	$1.86 - \frac{32.5}{f_c^{1/3} d_b}$	s_{max}	0.187mm
τ_{max}	$3.77 f_c^{1/3}$	τ_u	$3.1 f_c^{1/3}$
s_{max}	$0.17 f_c^{1/3} d_b$	s_u	$s_u = \frac{38.8}{f_c}$
k_1	$\frac{1.28\times10^3}{d_b}$	k_1	$k_1 = \frac{1.96\times10^3}{d_b}$
k_2	$1.38 f_c^{1/3}$	k_2	$\frac{0.64 f_c^{1/3}}{0.187 - 0.0016 f_c^{1/3} d_b}$
k_3	$\frac{29.6}{d_b f_c^{1/3}}$	k_3	$\frac{0.68 f_c^{1/3}}{38.8 f_c^{-1} - 0.187}$

CHAPTER 5
Adaptability of Proposed Crack Width Prediction Formulas

Last chapter estimated the value of each bond stiffness and characteristic points for both types of tri-linear model. Consequently, the tri-liner model can be draw by using the parameter of concrete strength (f_c) and bar diameter (d_b). The proposed crack width prediction formulas in chapter 3 can be calculated by those parameters as well.

This chapter presents the calculated crack width prediction formulas. The adaptability of calculated bond stiffness, tri-model and the calculated crack width comparing with test results are also discussed.

5.1 Bond Stiffness

Table 5.1 shows the comparison of calculated bond stiffness with the experiment ones for the non-coated type AFRP bar specimens. In general, the calculated k shows a good agreement with the experiment ones. Regarding to the specimen reinforced with the non-coated type bar, the max. bond stress of those splitting specimens are considered as the value of splitting bond stress. It can be said that the max. bond stress does not have a large influence on the initial bond stiffness. However, they influence the k_2 and k_3 as show in Table 5.1 (b) and Table 5.1 (c), respectively. For those sand-coated type bar reinforced specimen, the variation of τ_{max} influences both k_2 and k_3.

Table 5.1 (a) Comparison of the calculated k with the experiment ones
(Non-coated type, k_1)

Specimen	Cal. k_1 (N/mm^3)	Exp. k_1 (N/mm^3)	Cal. k_1 / Exp. k_1	Failure mode
C24RA9	131.7	151.0	0.87	Pullout
C36RA9	131.7	167.5	0.79	Pullout
C48RA9	131.7	154.0	0.86	Pullout
C24RA11	117.0	100.8	1.16	Concrete splitting
C36RA11	117.0	110.1	1.06	Pullout
C48RA11	117.0	140.6	0.83	Concrete splitting
C36RA7	158.1	128.7	1.23	Pullout
C36RA13	94.8	112.2	0.84	Concrete splitting

Table 5.1 (b) Comparison of the calculated k with the experiment ones
(Non-coated type, k_2)

Specimen	Cal. k_2 (N/mm^3)	Exp. k_2 (N/mm^3)	Cal. k_2 / Exp. k_2	Failure mode
C24RA9	4.21	5.16	0.82	Pullout
C36RA9	4.62	4.08	1.13	Pullout
C48RA9	5.02	5.38	0.93	Pullout
C24RA11	4.21	7.23	0.58	Concrete splitting
C36RA11	4.62	3.31	1.40	Pullout
C48RA11	5.02	12.25	0.41	Concrete splitting
C36RA7	4.60	5.27	0.87	Pullout
C36RA13	4.60	3.99	1.15	Concrete splitting

Table 5.1 (c) Comparison of the calculated k with the experiment ones
(Non-coated type, k_3)

Specimen	Cal. k_3 (N/mm^3)	Exp. k_3 (N/mm^3)	Cal. k_3 / Exp. k_3	Failure mode
C24RA9	1.00	0.96	1.04	Pullout
C36RA9	0.91	0.68	1.34	Pullout
C48RA9	0.84	0.88	0.95	Pullout
C24RA11	0.89	1.65	0.54	Concrete splitting
C36RA11	0.81	1.03	0.79	Pullout
C48RA11	0.74	3.06	0.24	Concrete splitting
C36RA7	1.10	1.22	0.90	Pullout
C36RA13	0.67	2.07	0.32	Concrete splitting

Table 5.1 (d) Comparison of the calculated k with the experiment ones
(Sand-coated type, k_1)

Specimen	Cal. k_1 (N/mm^3)	Exp. k_1 (N/mm^3)	Cal. k_1 / Exp. k_1
C24RA9S	201.5	235.3	0.86
C36RA9S	201.5	228.0	0.88
C48RA9S	201.5	217.0	0.93
C24RA11S	179.1	177.3	1.01
C36RA11S	179.1	140.6	1.27
C48RA11S	179.1	152.0	1.18
C36RA7S	242.1	222.3	1.09
C36RA13S	145.2	145.6	1.00

Table 5.1 (e) Comparison of the calculated k with the experiment ones
(Sand-coated type, k_2)

Specimen	Cal. k_2 (N/mm^3)	Exp. k_2 (N/mm^3)	Cal. k_2 / Exp. k_2
C24RA9S	14.87	14.64	1.05
C36RA9S	16.87	17.23	0.98
C48RA9S	18.95	25.76	0.74
C24RA11S	15.54	12.86	1.21
C36RA11S	17.72	10.35	1.71
C48RA11S	20.04	14.71	1.36
C36RA7S	15.77	16.06	0.98
C36RA13S	19.72	11.31	1.74

Table 5.1 (f) Comparison of the calculated k with the experiment ones
(Sand-coated type, k_3)

Specimen	Cal. k_3 (N/mm^3)	Exp. k_3 (N/mm^3)	Cal. k_3 / Exp. k_3
C24RA9S	1.77	2.15	0.82
C36RA9S	2.69	2.50	1.08
C48RA9S	4.00	2.32	1.73
C24RA11S	1.77	1.50	1.18
C36RA11S	2.69	2.91	0.93
C48RA11S	4.00	3.10	1.29
C36RA7S	2.65	2.97	0.89
C36RA13S	2.65	1.34	1.84

5.2 Crack Width Prediction Formula

Using the estimated parameters in Chapter 4, the crack width prediction formula can be calculated. Based on the definition of tri-linear model, the positive or negative of k is automatically determined. Therefore, only need to calculate Eq. (3.1), Eq. (3.2), Eq. (3.5) and Eq. (3.9).

5.2.1 Crack width prediction formula for non-coated type

The crack width prediction formula for non-coated type is given as:

$$w_{cr} = 2 \cdot \sqrt{\frac{\sigma_{ct} A_c}{641\pi}\left(\varepsilon_l - \frac{1+np}{2} \cdot \frac{\sigma_{ct} A_c}{E_b A_b}\right)} \qquad \left(w_{cr} < 0.07\text{mm}\right) \qquad (5.1)$$

On the other hand, one of the part of formula can be simplified as:

$$\frac{1+np}{2}\cdot\frac{\sigma_{ct}A_c}{E_bA_b}=\frac{1}{2}\cdot\frac{\sigma_{ct}A_c}{E_bA_b}+\frac{\sigma_{ct}}{2E_c}\cong\frac{1}{2}\cdot\frac{\sigma_{ct}A_c}{E_bA_b}=\frac{1}{2}\cdot\frac{\sigma_{ct}}{E_bp}\quad\left(\because\frac{\sigma_{ct}}{2E_c}\approx 0\right) \tag{5.2}$$

The simplified calculated formulas can be presented as:

$$w_{cr}=2\cdot\sqrt{\frac{\sigma_{ct}A_c}{2.01\times10^3}\left(\varepsilon_l-\frac{\sigma_{ct}}{2E_bp}\right)}\qquad\left(w_{cr}<0.07\text{mm}\right) \tag{5.3}$$

$$w_{cr}=2\cdot\left\{0.035-\frac{32.5}{\alpha}+\sqrt{\frac{1.45\sigma_{ct}A_c}{\alpha\pi}\left(\varepsilon_l-\frac{\sigma_{ct}}{2E_bp}\right)+\frac{1.06\times10^3-1.14\alpha}{\alpha^2}}\right\} \tag{5.4}$$

$$\left(0.07\text{mm}<w_{cr}<3.72-\frac{32.5}{\alpha}\right)$$

$$w_{cr}=2\cdot\left\{\left(1.86-\frac{32.5}{\alpha}-0.085\alpha f_c^{\,1/3}+\sqrt{\frac{f_c^{\,1/3}\sigma_{ct}A_c}{46.6}\left(\varepsilon_l-\frac{\sigma_{ct}}{2E_bp}\right)+0.007\alpha^2-\frac{0.062f_c+49.2d_b}{\alpha}-0.155d_bf_c^{\,2/3}}\right\} \tag{5.5}$$

$$\left(3.72-\frac{32.5}{\alpha}<w_{cr}<0.34\alpha\right)$$

Where,

Coefficient $\alpha=f_c^{\,1/3}d_b$

5.2.2 Crack width prediction formula for sand-coated type

The crack width prediction formula for sand-coated type is given as follows.

$$w_{cr} = 2 \cdot \sqrt{\frac{\sigma_{ct} A_c}{3.08 \times 10^3} \left(\varepsilon_l - \frac{\sigma_{ct}}{2 E_b p} \right)} \qquad \left(w_{cr} < 0.0032 f_c^{\,1/3} d_b \right) \tag{5.6}$$

$$w_{cr} = 2 \cdot \left\{ 0.00942\alpha - 0.914 + \sqrt{\frac{3.13 \sigma_{ct} A_c \beta}{\alpha \pi} \left(\varepsilon_l - \frac{\sigma_{ct}}{2 E_b p} \right) + 23.9 \beta^2 - 0.00781 \alpha \beta} \right\} \tag{5.7}$$

$$\left(0.0032 f_c^{\,1/3} d_b < w_{cr} < 0.374\text{mm} \right)$$

$$w_{cr} = 2 \cdot \left\{ \frac{215}{f_c} - 0.85 + \sqrt{\frac{(0.55 f_c - 114) \sigma_{ct} A_c \beta}{f_c \alpha \pi} \left(\varepsilon_l - \frac{\sigma_{ct}}{2 E_b p} \right) + \frac{4.62 \times 10^4}{f_c^{\,2}} - \frac{372}{f_c} - \frac{0.324 d_b}{f_c^{\,2/3}} - 0.0016\alpha + 0.721} \right\} \tag{5.8}$$

$$\left(0.374\text{mm} < w_{cr} < \frac{77.6}{f_c} \right)$$

Where,

Coefficient $\alpha = f_c^{\,1/3} d_b$

Coefficient $\beta = 0.187 - 0.0016 f_c^{\,1/3} d_b$

5.3 Calculated Tri-Linear Model

The comparison of calculated tri-linear model with the bond – stress relationship from test result are shown in Fig. 5.1.

The calculated tri-linear model matches the curve well except two series of specimen reinforced with non-coated type of AFRP bar which failed by concrete splitting. As discussed in Chapter 4, the concrete strength does not have a large influence on the τ_{max}. However, C24RA11, C48RA11 and C36RA13S series show a large variation of bond stress.

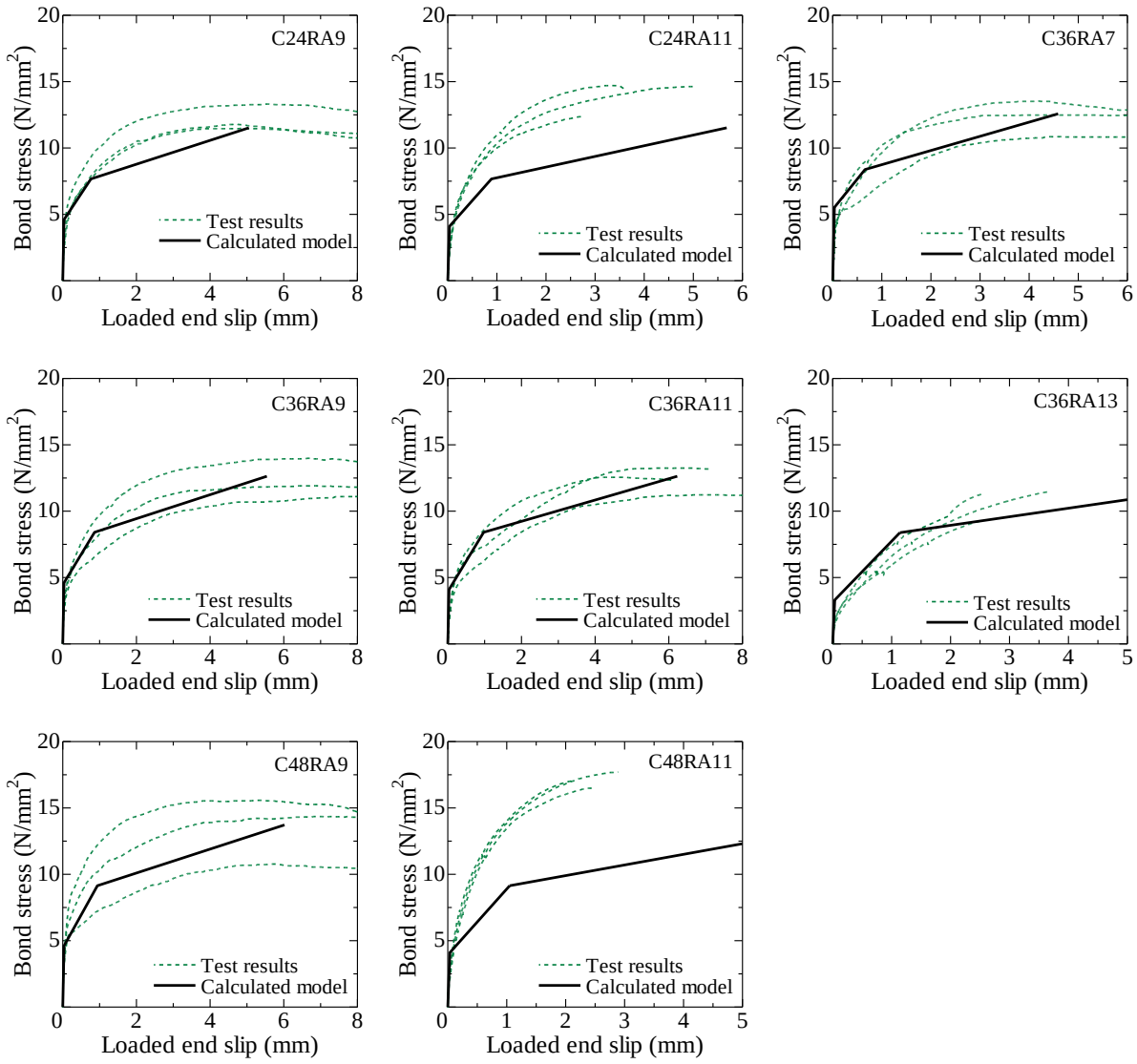

Fig. 5.1 (a) Calculated tri-liner model for non-coated type bar specimen

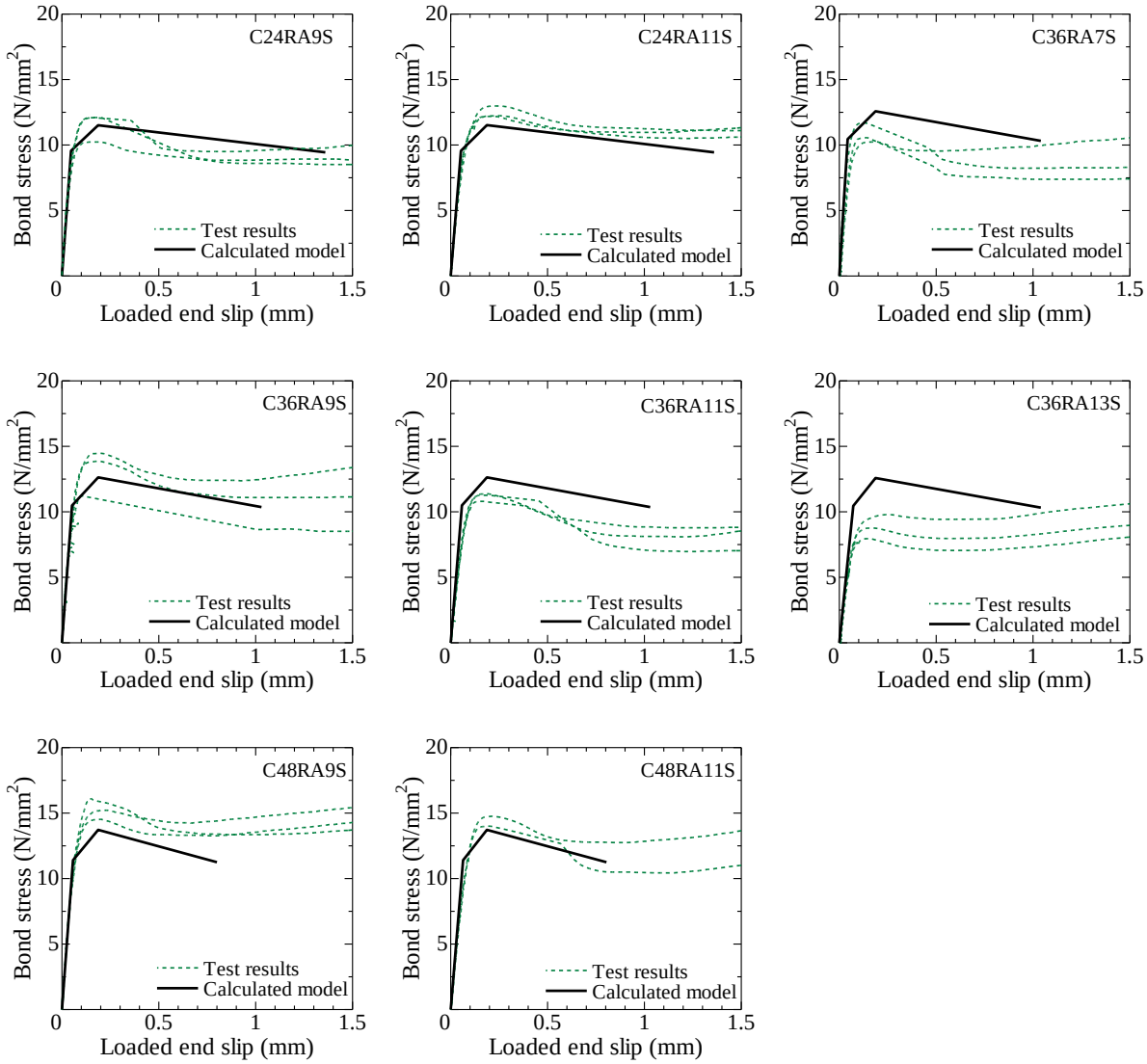

Fig. 5.2 (b) Calculated tri-liner model for sand-coated type bar specimen

5.4 Adaptability of Calculated Prediction Formulas

The comparison of the predicted crack width with that observed in tensile bond test are shown in Fig. 5.2. It also shows the range of the curve calculated by k_1, k_2 or k_3. The experimental reinforcement strain is obtained by the tensile load divided by the sectional area and elastic modulus of tested AFRP bar.

In general, the prediction formulas work well with the non-coated type series. However, some of the sand-coated type series show a deviation from the experimental curves. It is considered that perpendicular cracks in tensile bond test affect the experimental measured crack width in those specimens.

Regarding to the calculated prediction curve, the range calculated by k_1 is too small because at the first increase branch the bond performance is very well which means a high bond stress with a little slippage.

For both types of specimens, the crack width is mainly depended on k_2 and k_3. On the other hand, some of the sand-coated type series specimens with the small s_u cannot provide a relatively enough calculation range.

Comparing with the tri-linear model and the prediction crack width, it can be said that a good bond performance leads less crack width at the same level of reinforcement strain.

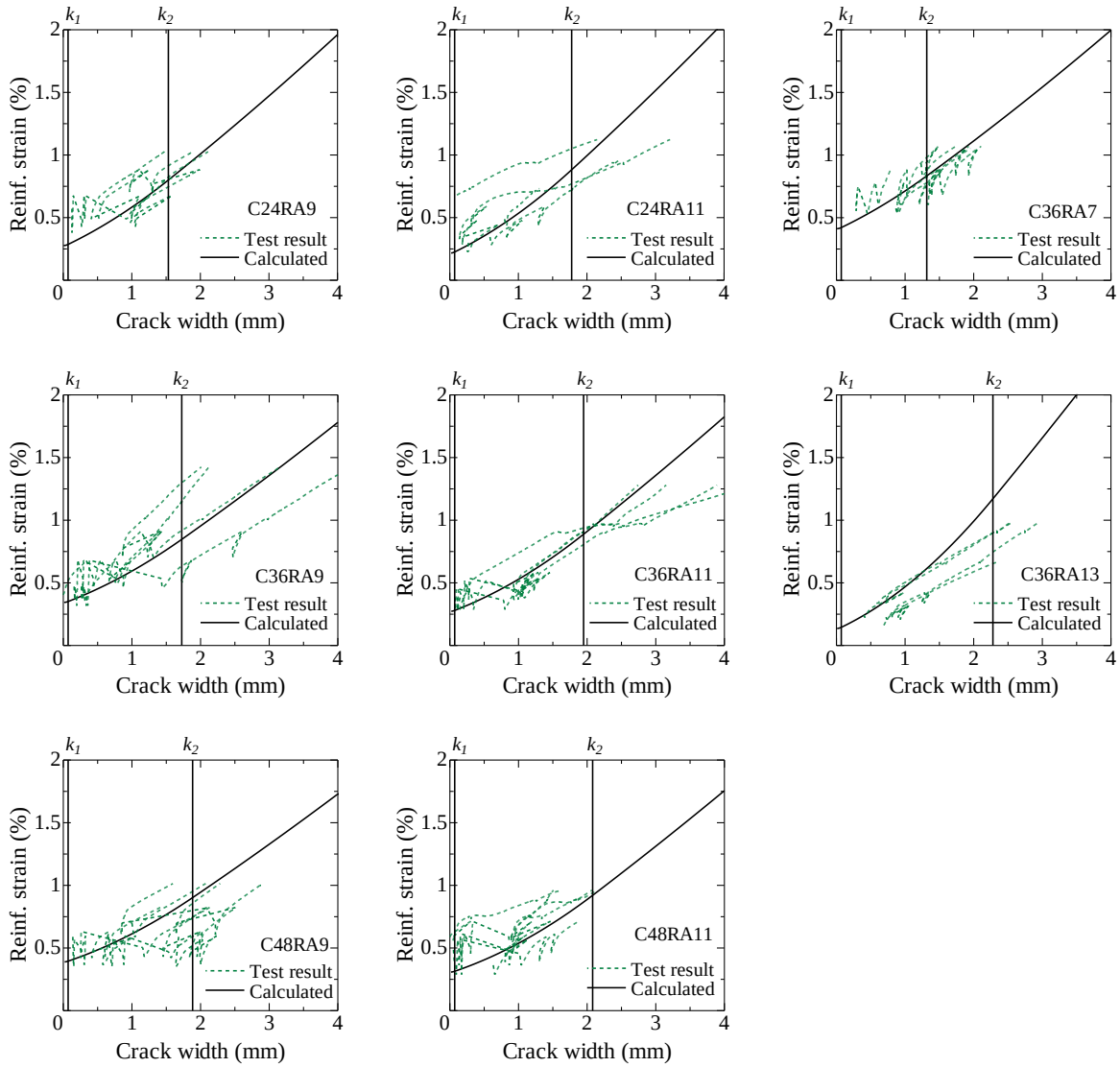

Fig. 5.3 (a) Crack width – reinforcement strain relationship
(Non-coated type bar specimen)

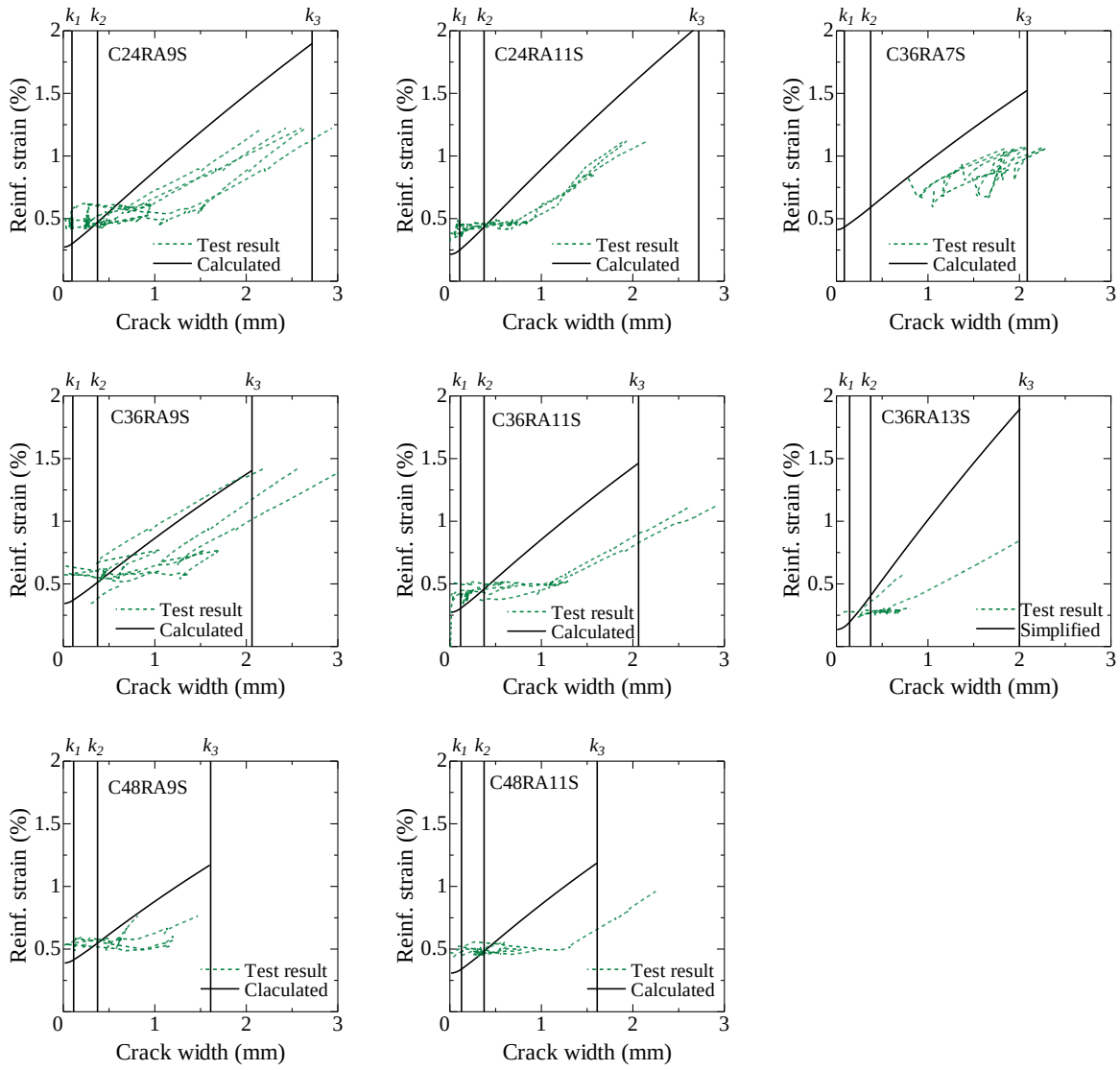

Fig. 5.4 (b) Crack width – reinforcement strain relationship
(Sand-coated type bar specimen)

CHAPTER 6 Conclusions

In this study, two types of tri-linear models for bond constitutive law are proposed based on the experimental results of pullout bond test both for non-coated type and sand-coated type AFRP bars. Under the regression analysis of the pullout bond test results, each of the bond stiffness and characteristic value is estimated as a function which is mainly related to concrete strength and bar diameter.

The crack width prediction formulas, that are given by the relationship between the reinforcement strain and loaded end slip which is equal to half of the crack width, has been proposed by using the estimated bond constitutive law. The proposed crack width prediction formulas show good agreements with the experimental crack widths.

In addition, the followings are found during the pullout bond test.

1. Surface treatment of the braided AFRP bars largely affects the bond constitutive law. However, surface treatment has little influence to the max. bond stress as the max. bond stress of both types are similar in case of same conditions.

2. Concrete strength does not have a large influence on the max. bond stress or slipping bond stress and slippage at those stresses for both types of AFRP bar.

ACKNOWLEDGEMENTS

I would like to express my deepest appreciation to my supervisor, Professor Toshiyuki Kanakubo for his insightful comments and suggestions, kindly communication and carefully proofreading the manuscript during the research project over years.

I would also like to thank my co-research advisors, Associate Prof. Gaku Shoji and Associate Prof. Akira Yasojima for their valuable suggestions and constructive comments on my study.

I would also like to acknowledge the technical staff member, Mr. Kojima. Without his support for the experiment this thesis could not have been completed.

I also thank all the members of F115 laboratory to give me the best environment to do the research, especially Ms. Okazaki HITOMI who help me carrying out the experiment a lot and Mr. Yu MU who give me many advises for living abroad as foreign student.

Special thanks to Fibex Co., Ltd for providing the experiment materials.

REFERENCES

1-1) Nanni A., De Luca A., Zadeh HJ. Reinforced Concrete with FRP Bars: Mechanics and Design, CRC Press, 2014.

1-2) Rehm, G., Über die Grundlagen des Verbundes zwischen Stahl und Beton, Deutscher Ausshcuss für Stahlbeton, H. 138, 1961.

1-3) Kanakubo T., Yamato N., Crack Width Prediction Method for Steel and FRP Reinforcement Based on Bond Theory, Journal of Advanced Concrete Technology, Vol. 12, No. 9, pp. 310-319, 2014.